

# Penrose platter spin ices - Artificial magnetic quasicrystals

Jonathan Kelsey

April 29, 2013

### **Abstract**

Analysis of the seven vertex Penrose model, to describe artificial spin ice, via an Ising spin system with long range dipolar interactions, evolving by local stochastic dynamics. Some evidence for a phase transition was attained and an exploration of a potential ground state discussed.

# Contents

0.1	Introduction . . . . .	2
0.1.1	Interest . . . . .	2
0.1.2	Literature review . . . . .	2
0.1.3	Intentions . . . . .	6
0.2	Method . . . . .	7
0.2.1	Discretisation . . . . .	7
0.2.2	Hamiltonian simplification . . . . .	8
0.2.3	Monte Carlo specifics . . . . .	8
0.2.4	Penrose distribution . . . . .	9
0.2.5	Software . . . . .	10
0.2.6	Statistical analysis . . . . .	10
0.2.7	Square ice test case . . . . .	11
0.3	Monte Carlo simulation and statistical analysis of Penrose ASIs . . . . .	14
0.3.1	Vertex classification and entropy . . . . .	14
0.3.2	720 dipole system . . . . .	15
0.3.3	1650 dipole system . . . . .	20
0.3.4	Limiting case MC . . . . .	25
0.4	Conclusion . . . . .	28
0.5	Appendix . . . . .	28

# 0.1 Introduction

## 0.1.1 Interest

This topic relates to the energy landscape of magnetic dipole interactions of a system with frustrated geometry arising from Penrose geometry. Of late artificial spin ice systems with frustrated geometry and Ising-like interactions have attracted interest. This research is generally inspired due to emergent phenomena and low temperature behaviour which arise within these essentially classical condensed matter systems, such as the formation of quasi-particles with net magnetic charge known as monopoles [3]. The insight gathered with the implementation of artificial spin ice systems such as the efforts by R.F. Wang and C.Nisoli [25] has motivated greater study. Moreover the discovery of quasi-crystals led to Dan Shechtman receiving the 2011 Nobel Prize in chemistry [11].

## 0.1.2 Literature review

In the first section I explore the phenomena of frustration, and consider how it applies to water ice. Subsequently I will discuss spin ices and spin glasses. Next I will introduce the concept of artificial spin ice systems realised within contemporary condensed matter experiments. Magnetic quasicrystals will be explored before finally moving on to the Monte Carlo Method.

### Frustration

A system is said to be frustrated when competing interactions cannot all be satisfied simultaneously [25]. Magnetic spin systems with frustrated geometry can lead to exotic low temperature system states, an example of which is the spin ice system, which is analogous to the frustration of hydrogen ions in water ice [25]. In a particular square lattice (see figure 1) an anti-ferromagnetic configuration is achievable where each spin is anti-aligned with its immediate neighbours, thus neutralizing long distance net magnetisation. The simplest lattice structure to demonstrate frustration is a triangle lattice. Once two adjacent dipoles have anti-aligned the third spin cannot anti-align with both; it can only align with one and anti-align with the other. The energy of these two configurations is the same and equivalent states exist in different orientations for the three vertices, thus the ground state is 6 fold degenerate [17]. Such a system will never achieve perfect order even at absolute zero; the system has residual entropy. As the ground state energy is degenerate, equivalence is drawn for phase states analogous to water and ice within magnetic spin systems [25].

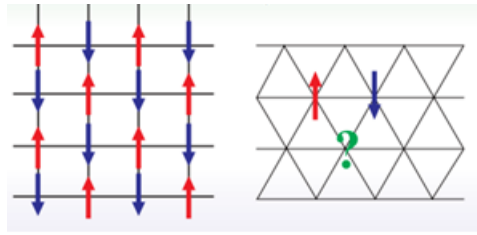


Figure 1: Frustrated (right) and un-frustrated (left) lattices. Adapted from figure 1 of reference [17]

### Water ice

The phenomenon of frustration was initially studied in the context of water ice which exhibits residual entropy. Calorimetric measurements of water ice by W. F. Giaque et al resulted in a calculation of entropy which differs from the result theoretically obtained result for an ideal gas [7]. The variance was explained by Linus Pauling, who showed that ice possess a finite entropy even at absolute zero with a value 3.4 J/(molK) accounting well for the difference [19]. In the solid phase of water, oxygen ions form a tetrahedral basis, where every oxygen atom is surrounded by four hydrogen ions. The hydrogen atom coupled with each oxygen atom, the separation of charge forms an electric dipole. There are  $2N$  hydrogen atoms per  $N$  oxygen molecules [19]. The states that form the minimum spin interaction potential are known as the two in two out configuration. Where two hydrogen atoms are close to the oxygen atom at the central vertex and two are near adjacent oxygen atoms. The 'two in two out' configuration is also known as an ice rule which accounts for the arrangement of water atoms in ice. [25] Spins in a tetrahedron cannot be simultaneously anti-aligned just like the triangular lattice.

In general moments align when they point in the direction of a common axis, on the contrary moments which are off-axis conform such that their projections to that axis anti-align. The reason for this behaviour lies with the dipole-dipole interaction energy, quantified with the classical interaction Hamiltonian:

$$U(\mathbf{r}_{12}) = \frac{\mu_0}{4\pi} \frac{1}{r_{12}^3} \times [\mathbf{m}_1 \cdot \mathbf{m}_2 - \frac{3(\mathbf{m}_1 \cdot \mathbf{r}_{12})(\mathbf{m}_2 \cdot \mathbf{r}_{12})}{r_{12}^5}] \quad (1)$$

Adapted from reference [16] Where  $r_{12}$  is the magnitude of the vector connecting dipoles moments  $\mathbf{m}_1$  and  $\mathbf{m}_2$ .

Water exists with many distinct thermodynamic phases which can be viewed with a phase diagram of P,V and T. Within these diagrams critical points exist where phases can co-exists at specific points. The phase diagram of water is in essence a concise collection of phase change data which is the summation of

experimental knowledge about the different forms in which water can take.

### Spin ice and glass

A spin glass is a frustrated magnetic system where the dipole moments are distributed and oriented randomly. These systems exhibit no long range order of the anti-ferromagnetic or ferromagnetic type [2]. A spin ice features spins placed on a regular lattice, with ordered orientation, however the orientation of the spin has an associated polarity, which can flip its direction. These systems can display long range order if geometrical frustration is absent [8]. A spin-ice should be thought of as an ordered structure, whereas a spin glass is essentially disordered. In a frustrated spin ice the overall material is magnetic as the dipole interactions are not capable of eliminating net magnetisation. A spin glass is non-magnet as all the dipoles orientations are randomly distributed. RKKY, coupling oscillates with distance between anti and ferromagnetic states. Competing interaction and frustration leads to a different form of frustration. [2] Perhaps a structure can exist with intermediary features such as quasi-periodic crystal resulting from Penrose tiling geometry which has aperiodic spin locations but ordered spin orientations.

### Artificial spin ice (ASI)

Spin remains a difficult topic to experimentally probe in real world systems such as water. The desire to comprehend the dynamics of spin ices required emulating the behaviour artificially using condensed matter apparatus. The spin degrees of freedom in spin ice are supplanted with miniature magnets created at microscopic length scales. Although the magnets are nano-scale classical physics is still suitable in explaining their dynamics.

Fabrication of these devices is a four step process. Firstly a substrate with a resist is prepared. Next EBL (Electron beam lithography) an etching technique selectively removes some of the resist exposing some of the substrate. After exposure new material(permalloy) is added via sputtering or evaporation. Finally the resist is dissolved leaving just permalloy in place. [20]

2d nanostructures composed of single domain ferromagnetic islands can be made with arbitrary geometry, in order to investigate systems analogous to spin ices. Emulation is possible as the magnetic anisotropy of permalloy is essentially zero thus the magnetic moment is forced to align along the longer axis of the nano-magnet resulting in a system much like the Ising spin system [25].

The microstate of an ASI can evaluated directly with MFM(magnetic force microscopy.) One can in-

dividually probe each nano-magnet for its moment and by measuring all the islands the global microstate can resolved [25].

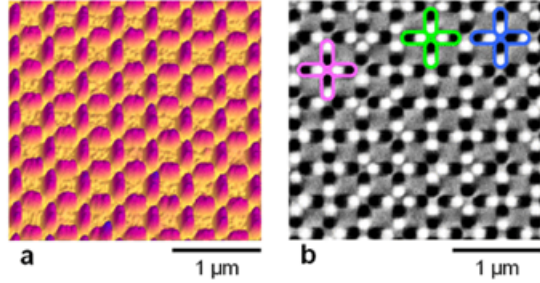


Figure 2: Adapted from figure 2 reference [25], left is an atomic force microscope image of the surface topology of an ASI system, right is an MFM image of the magnetic interaction of the ASI with a magnetic read head.

The arrangement of spins in an ASI (the magnetisation) can be quantified with an order parameter. An order parameter is used in statical mechanics to differentiate two phases with different order, typically it is defined to be zero in one phase and non-zero in another. Divergence of the variance of the order parameter is usually indicative of approaching a critical point in the systems phase diagram [21].

The order parameter can be determined by comparing the polarisation of the dipoles to a ground state mask. It is accomplished through multiplying the spin polarization of a state with its counter part in the mask and divided by the total number of spins. Thus revealing a property which will be  $\pm 1$  for a system with perfect mask order and 0 for perfectly disordered state. It is not important as to whether the state perfectly aligns or anti-align to the mask as each of these states have the same order thus the absolute value of the parameter is taken.

The merit of ASI is that the interactions within the system can be tuned by applying a magnetic field or via modifying the lattice parameters prior to the ASI's fabrication.

ASI systems as indicated before can yield emergent properties such as monopoles which exist as quasi-particles with net magnetic charge expressed within many-body system with strong interactions. The existence of the phenomena purportedly explains the mysterious phase transition from a liquid like to gas like state within spin ice systems with an externally applied magnetic field [3].

### Square lattice spin ice

Square spin ice can be decomposed into 16 vertices which can be organised into four topological groups with the same energy.

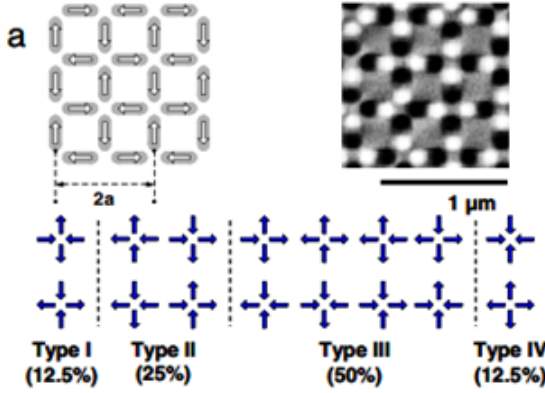


Figure 3: Vertex classification of a square ASI, organised with ascending energy. Reference [5] figure 1.

The square lattice has two distinct states of order. The distribution can be in a ferromagnetic configuration this is where the individual dipole moments of the add constructively creating a macroscopic magnetic field that is measurable. In this state of order the composite vertices are in the first excited state.

Another state of order available to the system is the anti-ferromagnetic state, this is where spins destructively add yielding no net magnetisation. This state is the ground state of the system as each vertex is in the lowest energy configuration. The anti-ferromagnetic state exists at temperatures below the Nel temperature, above this temperature most systems exhibit paramagnetism. [29] The groundstate is doubly degenerate as by flipping every spin in the system does not affect the global energy.

In between these two states of order lies disordered states with configurations known as a spin liquid. [15]

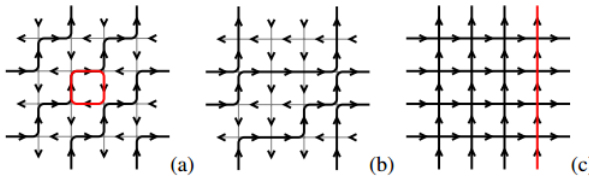


Figure 4: Characteristic phases of the sixteen-vertex model on the square lattice. (a) Antiferromagnetic (AF) order. (b) Collective spin liquid (SL) phase. (c) Frozen ferromagnetic (FM) order. Reference [15] figure 2.

Thermal phase transition of square spin ices have been investigated with Monte Carlo simulations, employing single spin flip transitions, ignoring interactions beyond nearest neighbours. Comparisons to real data yield convincing correlations. The micro-state with minimised interaction energy follows the two in

two out ice rules just like real water ice with a pyrochlore lattice [15].

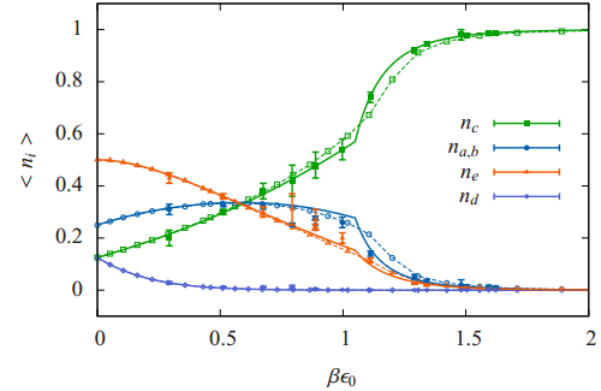


Figure 5: Average densities of different vertex types as a function of  $\beta\epsilon_0$ . Full symbols with error bars are experimental data. Empty symbols with dotted lines correspond to the equilibrium Continuous Time set-up data. The cluster variational mean-field Bethe-Peierls analytic solution of the sixteen-vertex model is shown in solid lines. Reference [15] figure 5.

An order parameter for the square spin ice consists of comparing each spin in the state to the known ground state configuration, which is the anti-ferromagnetic state depicted in figure 4.

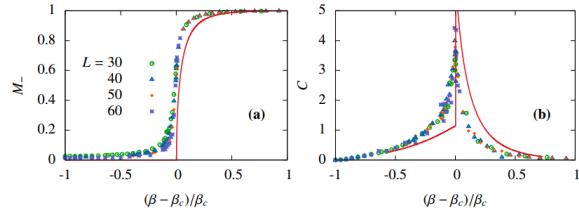


Figure 6: Reference [15] figure 6. Statistical analysis of the variance of energy were used to calculate the heat capacity of the square spin ice (right). The magnetisation order is depicted (left)

## Magnetic quasicrystals

The discovery of Quasicrystal has changed the field of crystallography forever. A Quasicrystal or quasi-periodic crystal has an ordered but a non-periodic structure, that is to say it has no translational symmetry. Quasicrystals can possess rotation symmetry e.g. 5 fold symmetry. These structures do display long range orientational order and thus can undergo Bragg diffraction [22].

The magnetic behaviour of quasicrystals are currently poorly understood, quasi-crystalline alloys have been shown to demonstrate a vast array of different magnetic behaviours including diamagnetism,

paramagnetism, ferro-magnetism and spin-glass properties [9]. Antiferromagnetic structures on regular lattices have been thoroughly examined via experiments and are well understood. Antiferromagnetic ordering in quasicrystals is still disputed in the literature. Spin-glass like spin freezing have been observed in quasi-crystals at low temperatures made of rare earth materials although their exact dynamics do differ from conventional spin glass like materials. Antiferromagnetic coupling on various quasicrystals (including Penrose quasicrystals) were investigated and conclusions draw indicating that frustration is intrinsic. [23].

### Penrose quasicrystal lattice

Apart from proving local frustration in quasi-crystals information about Penrose spin ice quasicrystals in the literature is quite sparse. Within Leeds university some research has been conducted in this area. Via personal communication with PhD student Dong Shi I have gathered some insight into the system.

The penrose distribution can be decomposed into seven topologically unique vertex classes each with many possible energetic configurations. On investigation of the vertices, Dong Shi managed to find a partial and doubly degenerate anti-ferromagnetic configuration with zero net magnetization. He arrived at this configuration by examining the ground and first excited states of the vertex classes. He noticed that two of the seven classes had a relatively small energy gap between the ground and first excited states. The state was sought which maximised the number of vertex classes in the lowest energetic type. However as the Penrose is intrinsically frustrated all vertex types cannot be simultaneously in the ground state. A compromise had to be made, the classes with the lowest energy gap were allowed to have some or all of their population in the first excited state.

The mask can be split into two parts, the first part known as the skeleton mask involves all the dipoles which are not coloured yellow or purple. The remnant part of the mask without the purple dipoles are known as flip islands.

Nearest neighbour interactions where assumed to be the only energetically significant contributions. The configuration of the vertex island in relation to each other, may in fact have long range interaction contributions, although this is currently unknown.

The production of Penrose ASIs was commissioned by Leeds university. The ASI was made by an external company, thus the growth temperature conditions are not well known. MFM was then used to evaluate the microstate of the spin ices as grown, also the samples were demagnetised by rotating them in a decreasing magnetic field.

It is not clear what is the correct order parameter

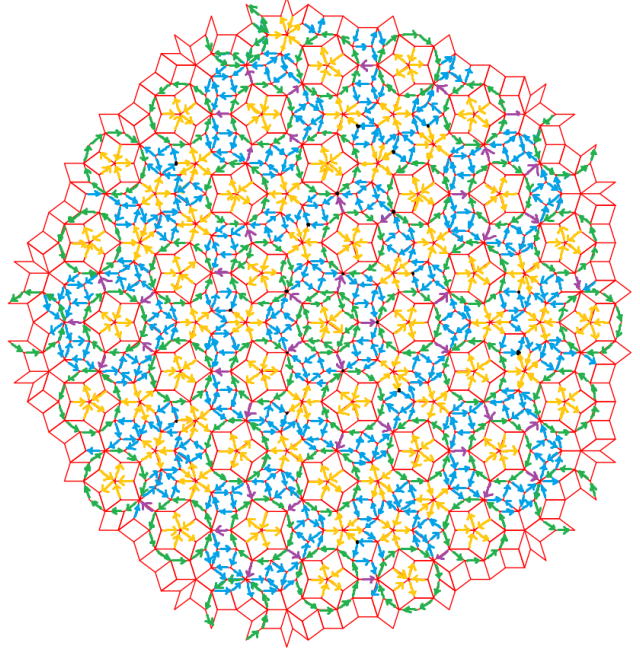


Figure 7: Colour coded diagram of a prospective ground state. Green and blue dipoles are fixed. Purple dipoles are independently free to flip without modifying the energy. Yellow colouring indicates that if every dipole member of this vertex island is flipped then the energy will not change. Image courtesy of Dong Shi.

for the Penrose system. One idea would be to compare the magnetic polarisation to a ground state such as the candidate which Dong Shi derived. One order parameter can be defined for the skeleton mask and one for the flip islands. The energetic configuration of the flip island relative to each other have not been sufficiently explored, in terms of their long range interactions, to be certain that they form the correct order parameter mask for this part of the system. Assuming Dongs anti-ferromagnetic skeleton mask one can atleast define a partial order parameter for the magnetisation depicted in figure 7.

During the growth of the sample at high temperature the magnetic islands are free to flip their dipole polarities. After growth the system will cool rapidly fixing the polarities of the dipoles. As the cooling experienced by the ASI after sample growth is unknown, it will be difficult to exactly replicate figure 8 with subsequent experiments or with synthetic data.

### Monte Carlo (MC)

The Monte Carlo method is a computational technique for sampling a distribution through the use of random numbers. The method rely upon the ergodic principle which states that time and ensemble averages are equivalent. Typically it is applied to a system

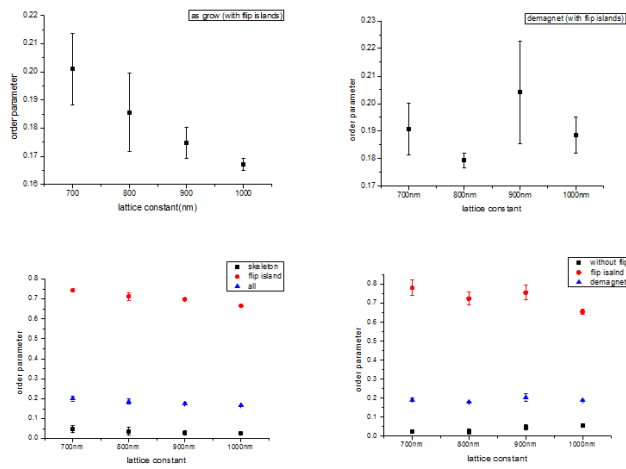


Figure 8: The skeleton mask and flip island magnetisation order parameters for the Penrose ASI samples in their as grown and demagnetised conditions. Courtesy of Dong Shi

that has too many possible configurations to compute them all in a reasonable time or for which analytic techniques are impossible [14].

The MC method acts as a simulated thermal bath, where local stochastic events emulate the random fluctuations present in real physical systems due to temperature. The utility of MC is that it allows the experimenter to have complete control over the temperature of the system and to use this control to investigate the different phases of matter which exist in said systems. By lowering the temperature in a suitable fashion most systems can be energetically minimised given sufficient time. Use of the Monte Carlo method is justified by the huge number of configurations of the Penrose system. A typical Penrose pattern has 1680 dipoles each with 2 spin configurations, thus the total number of configurations is  $2^{1680}$ , which is approximately  $5E + 505$ .  $5E + 505$  is a massive number considering there are estimated to be  $10^{80}$  atoms in the observable universe [18]. It is impossible to store all the possible configurations, thus the partition function cannot be known, it can however be estimated. The brute force method involves taking a collection of coordinates  $U(q^N)$ , calculating the proportional statistic weight  $\exp(-\frac{U(q^N)}{k_B T})$ , (where T is the temperature and  $k_B$  is Boltzmanns constant) this is then cached in store one. Next one calculates  $U(q^N) \exp(-\frac{U(q^N)}{k_B T})$  and caches it in store two. Most of the distinct  $q^N$  are iterated over while summing stores one and two. Finally store two is divided by one yielding an average expectation value for the energy.

$$\langle U \rangle = \frac{\sum_i U_i \exp(\frac{-\epsilon_i}{k_B T})}{\sum_i \exp(\frac{-\epsilon_i}{k_B T})}$$

The difficulties associated with this method include the fact that a large number of  $N$ s are require to get accurate averages, moreover many  $q^N$  will only make a small contribution to the running sum in store 2 [14].

The type of Monte Carlo I will employ to minimise the energy of a set of spin ice systems is called Metropolis Monte Carlo. Monte Carlo Metropolis avoids the problems associate with the brute force method. Initially one creates a configuration  $q_N$  and calculates the energy associate with it  $U(q_N)$ . Subsequently one modifies the distribution changing it in some fashion (in our case a dipole spin is flipped) to create a new distribution  $q_M$  and associate energy  $U(q_M)$ . The energy difference is then calculated  $dE = U(q_N) - U(q_M)$ . If the new state has lower configurational energy then it is accepted as the new configuration; else the state is conditionally accepted with an associated probability attributed to the Boltzmann factor  $P = \exp(\frac{-dE}{k_B T})$ . This equivalent to the probability associated with state N divided the probability of state M. If the energy difference of the two system states is zero, then the state is accepted with probability of unity. Otherwise as the energy difference approaches infinity, the probability of acceptance approaches zero. New configurations with lower energy will always be accepted. System states with greater but similar energy will likely be accepted. Local minima can be escaped as it is possible for the energy to increase but in general the system will precede to lower energy [14]. It is critical especially for a frustrated system that the minimisation technique allows escape from local minima which are plentiful in highly degenerate systems.

### 0.1.3 Intentions

The intention of this project is to use the computational technique Monte Carlo specifically the Metropolis algorithm to investigate the spin dynamics of both geometrically and magnetically frustrated systems via zero-field cooling. The model one will employ is an Ising like spin system with long range dipolar interactions evolving by local stochastic dynamics.

The resultant data can be analysed for statistical averages of quantities such as the energy and the populations of the component vertices in the system at various temperatures. Estimates for the heat capacity and magnetic susceptibility at various temperatures will be calculated where possible.

The two system geometries to be investigated are the square lattice geometry and the quasicrystal Penrose geometry.

Initially one will investigate the square geometry ice, it is a less complex system than the Penrose geometry and the ground state is known. Square spin ices have been studied extensively, with both synthetic computation and real world experimental data available for comparison.

It is prudent to test my methodology and see if it compares to the data available in the literature before moving on to the more complicated Penrose system.

On the successfully implementation and analysis of the square system, one will investigate the Penrose system.

One idea to investigate for the Penrose system, is to how modifying the lattice parameter affects the dynamics of the system. Another interesting property to investigate is how the system freezes as a function of thickness of the nano-magnets. Changing the thickness of a nano-magnet will change its moment altering its interaction energies. With further miniaturisation it may be possible to make small enough Nano-magnets that the system is able to thermally relax to a degenerate ground state. Such a system would unlikely be measurable through MFM technique as, if the system is susceptible to fluctuate at the thermal scale, then the magnetic read head of the MFM would certainly disrupt lower energy states of the system. Simulation is one way of avoiding the practical difficulties associated with probing such systems.

## 0.2 Method

### 0.2.1 Discretisation

In a real ASI each nano-magnet is a complex concatenation of many dipoles which interact via magnetic fields. Typical magnetic islands do not use cubic geometry as the dipole in said systems can in fact has 3-vector components and can point in any arbitrary direction. By making the island thinner in one axis one can start increasing the magnetic anisotropy confining it to the plane defined by the other two axes. Thinning one axis such as the thickness is simple via modifying the growth time during fabrication. To get the magnetisation ordered along a single axis requires reducing the width of the island such that it is extended in one direction and minimally expansive in the other

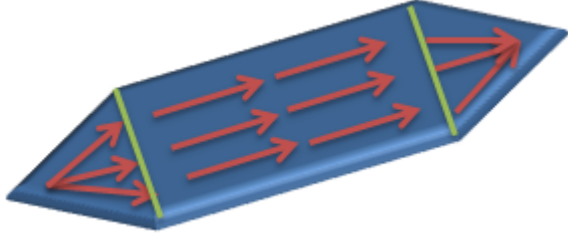


Figure 9: Figure to show a schematic of a magnetic nano-island. Dimension were taken to be 450nm along the major axis, with the square section being 200nm in length, by 80nm width and 26nm thick. Each nano-island was place between geometric vertices defined by the respective geometry chosen for the system. The geometric vertices are separated by 700nm (the lattice constant), thus each island does not span the entire length of the line defined by the two adjacent points.

Diamond shape islands is an attempt to force the magnetic field along one axial direction. The magnetisation nucleates within the central square island and expands outwards towards the tips. The convergence of dipoles towards the tip makes the components of along the width cancel and all that is left is a net dipole moment along the length of the island. This is an idealised interpretation as converging dipoles are left in an excited state at the tip and would energetically prefer to flip.

Monte Carlo simulation of ASI can be performed by coarse graining the systems in a suitable fashion. Instead of simulating each magnetic island as a complex arrangement of interacting dipoles, they can be approximated as a point dipole resulting in an Ising spin system. The magnitude of the dipole moment can be calculated from the volume of the island and the materials magnetisation saturation, with the assumption that the island is magnetically homogeneous. The magnetisation saturation for permalloy is  $7.96 \times 10^5 [Am^{-1}]$  [10] and the volume (for the dimensions given in figure 9) was determined to be  $5.46 \times 10^{-22} [m^{-3}]$  thus yielding a dipole moment of  $4.35 \times 10^{-16} [D]$ .

For the islands magnetisation to be saturated, it has to be coerced by a strong parallel field. The systems I will be investigating will be evaluated in their as grown configuration in which they have not been coerced by a field. The magnetisation saturation will be larger than the magnetisation found in a real system, thus the dipole moments and hence the calculated interaction energies may be overestimates. If it could be experimentally determined the degree to which these islands are saturated, then in principle a simple constant multiple would correct these energies and allow for comparison to physical experiments.

## 0.2.2 Hamiltonian simplification

To compute the interaction energy one will use the classical dipolar Hamiltonian equation 1 which is rewritten for convenience in the following form.

$$U(\mathbf{r}_{jk}) = \frac{\mu_0}{4\pi} \frac{1}{r_{jk}^3} \times [\mathbf{m}_j \cdot \mathbf{m}_k - 3(\mathbf{m}_j \cdot \hat{\mathbf{e}}_{jk})(\mathbf{m}_k \cdot \hat{\mathbf{e}}_{jk})] \quad (2)$$

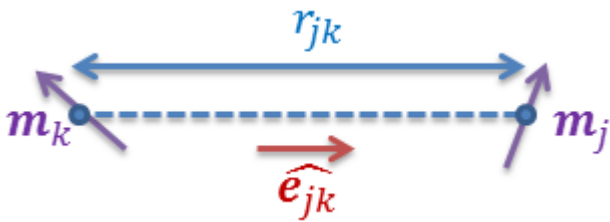


Figure 10: Schematic to show parameters of Hamiltonian.

In order to compute the interactions accurately it is sensible to factor out any small or large factors from the Hamiltonian. The dynamic parameter will be calculated in significant figures such that rounding errors will not pose an appreciable problem. The dipole moment can be expressed as  $\mathbf{m}_i = p_i \mathbf{M} V \hat{\mathbf{u}}_i$  where  $\mathbf{m}_i$  is the moment of the  $i$ th spin,  $p_i$  is the moments polarisation,  $\mathbf{M}$  is the homogeneous magnetisation of permalloy (assuming saturation),  $V$  is the volume of the island and  $\hat{\mathbf{u}}_i$  is the unit vector indicating the direction of the  $i$ th moment.

The dipole moments appear twice in the brackets and as such a common factor factor of  $(\mathbf{M}V)^2$  can be removed.

$$U(\mathbf{r}_{jk}) = \frac{\mu_0}{4\pi} \frac{(\mathbf{M}V)^2}{r_{jk}^3} \times [p_j p_k] [[(\hat{\mathbf{u}}_j \cdot \hat{\mathbf{u}}_k) - 3(\hat{\mathbf{u}}_j \cdot \hat{\mathbf{e}}_{jk})(\hat{\mathbf{u}}_k \cdot \hat{\mathbf{e}}_{jk})]] \quad (3)$$

The first part of equation 3 will only be multiplied at the end of the energy calculation, it is a common factor to all the interactions. The last bracket only has to be calculated once for each pairwise interaction and stored. Only  $[p_j p_k]$  has to be explicitly recalculated for each interaction energy update.

To work out all the interactions initially is an  $O(n^2)$  operation as each unique pair require computed values.  $O(n^2)$  operations are expensive but fortunately this only needs to be done once per simulation. After a list of interactions has been made updating a single flip is only  $O(n)$ . The flipped dipole will require updating its interaction to every other dipole but the interaction pairs which have not had members flipped do not require recalculation.

## 0.2.3 Monte Carlo specifics

Monte Carlo simulations will be performed on each system identified, in the hope of lowering the energy of the system and to observe the change in vertex population statistics.

MC will be used to perform single spin flips (a step), for  $n$  number of times per MC step, where  $n$  is the number of dipoles. For each MC step on average every dipole in the system will have had a chance to flip. Dipoles to be flipped were picked at random. The dipoles in the system will be initialised with randomised polarities to ensure their independence.

Changes in energy of a system will be determined initially at infinite temperature (every possible flip will be accepted regardless of it if yields a higher energy state) allowing the state space to be thoroughly explored. At infinite temperature occupation of states with equal degeneracy is equiprobable. By examining the degeneracy of the vertices of a system, one can infer their high temperature distribution.

A histogram of the population of energy changes can be plotted. The distribution data examined for interesting landscape features such as the stationary points. If the histogram is approximated as Gaussian; it is possible to define an effective energy that can be modified to adjust how the simulation explores the state space. To achieve this two energy changes are picked from the energy landscape, one close to the maximum  $dE_*$  and one close to the minimum  $dE_0$ . There is an associated probability with these energy changes,  $P(dE_0) = N$  where  $N$  is the probability read off the distribution at  $dE_0$  and  $P(dE_*) = N \exp(-\frac{dE_*}{k_B T})$ . If one sets the ratio of the probabilities to a constant  $\frac{P(dE_*)}{P(dE_0)} = \exp(-\frac{dE_*}{k_B T}) = 1/e$ , the effective energy is hence defined  $(k_B T)_* = dE_*$ . One can then define the system energy scale in terms of the effective energy  $k_B T = \alpha(k_B T)_*$  (where  $\alpha$  is modified to motivate the system into a higher or lower energy state as necessary.)

With the energy scale defined, one can perform MC simulations at finite temperature over a range of different  $\alpha$ 's. The distribution at each MC step will be analysed, the populations of each vertex class(VC) will be determined in terms of the identified class energy types (ET). The global energy will also be stored. The magnetisation order parameter will be determined where possible. For the square system the order parameter is calculated using the known ground state mask. For the Penrose system a partial order parameter will be obtained using the skeleton mask. Unfortunately hand coding all the dipoles in the skeleton mask was very time intensive, it was only done for one system type, the 1650 dipole Penrose pattern.

Multiple simulations will be run concurrently forming a simulation group. A simulation stage will con-

sist of running for a certain amount of MC time at a fixed temperature( $\alpha$ ). During each stage of constant temperature the system is in the canonical ensemble, and ensemble averages can be obtained from the statistics of that set. Once the distribution has had enough time to sufficiently equilibrate, setting a new  $\alpha$  can be considered. The vertex population averages of all concurrent runs within the group, along with their standard error multiplied by some constant, was used as the acceptance criteria for a transition to a new  $\alpha$ . The constant multiple was set to 0.5 for the square system to ensure that the simulation runs exit the stage with similar vertex populations. The Penrose system has seven times the number of VCs than the square type. Having the constant multiple of the standard error set to 0.5, resulted in an acceptance period which was too long to be practical, it was set to 2.5 to speed up the transition time. The method described is repeated over a range of  $\alpha$ 's.

Over the course of many simulations with different random initialisation states one should gain insight into the different states available in the lower energy region. If the system had smooth energy curvature one could use a Hessian matrix to look at stationary points within the surface and thus, through careful analysis, find the ground state. In a highly degenerate system(such as a Penrose ASI) the energy landscape is discontinuous and thus such a technique is not possible [24].

## 0.2.4 Penrose distribution

### Generation

Penrose patterns can be made using various techniques, the method I will be using is known as the projection method. For simplicity it will be described in detail in its 1-d formation.

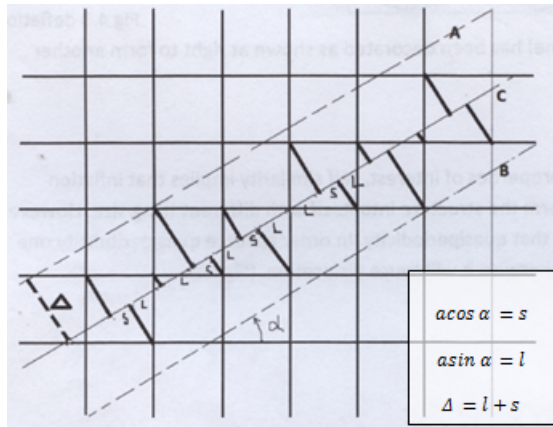


Figure 11: Generation of Fibonacci chain by segmentation of a 2-d grid onto a 1-d line [12].

Consider the two parallel dashed lines A and B su-

perimposed upon a grid with a displacement of  $2\Delta$ , in between the two lines is the solid line C. If lines A and B are projected perpendicular to the angle , from the vertices of the square grid to the solid line C, one derives line segments defined by a discrete set of points. If the slope C is irrational then the segments obtained form a Fibonacci chain. In other words if the line cutting the 2-d grid never touches a vertex then the line segments is aperiodic. Moreover this condition satisfies the golden ratio. The grid is defined by the lattice parameter  $a$  [6].

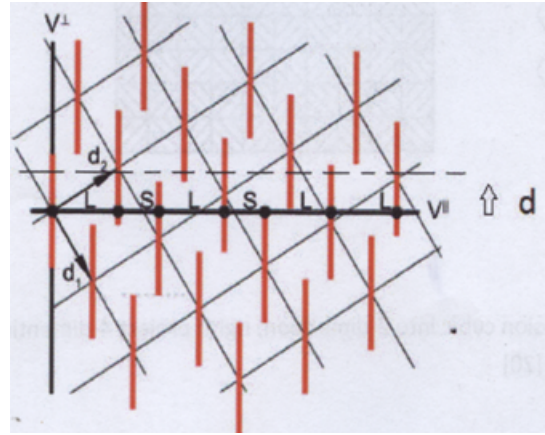


Figure 12: Generation of a Fibonacci chain by projection of a 2-d grid onto a 1-d line where the segmented line now forms the axis [12].

Now consider the same arrangement where instead the line slope C forms the horizontal axis. Different Fibonacci chains can be formed by moving a distance  $d$  from the horizontal axis.

This demonstration indicates that a quasi-periodic 1D pattern can be formed by projecting a uniform 2D grid on to a 1D line, so long as the grid or equivalently the line is irrational. On the other hand if the grid/line is rational a periodic 1D pattern is formed.

The projection technique can be generalised to higher dimensions, although intuition becomes difficult. By intersecting a 5D cubic lattice with a 2D plane, and looking at the cubes with points in common with the plane, one can project the cube centres onto the plane revealing vertices of a rhombus [p40] [27]. By increasing the dimension of the subtending plane to 3D, a projection from 5D a grid to 2D will instead form a 2D Penrose pattern [6].

The project technique can be better understood in terms of its mathematics. Consider a cubic lattice in  $n$ -dimensions  $R^n$ , now consider an orthogonal vector  $d_i$  which spans the space.  $R^n$  may be split into subspaces  $R^m$  and  $R^{n-m}$ , likewise vector  $d_i$  may be broken in two vectors forming  $p_i$  and  $q_i$  which span the subspace. If lattice points  $r = \sum_{i=1}^n h_i d_i$  are projected in to  $R^m$  then we are left with the projected

point  $s = \sum_i h_i p_i$ , equivalently if  $r$  is projected into subspace  $R^{n-m}$  we are left with  $t = \sum_i h_i q_i$ . The condition for aperiodicity is to confine  $t$  to lie inside volume  $V = \sum_i \lambda_i q_i$  where  $0 < \lambda_i < 1$ . Point  $s$  hence forms a quasi-periodic pattern in  $R^m$ . To get a 2 dimensional aperiodic pattern  $d = 5$  and  $m = 2$ . For a Penrose pattern the volume condition must be modified to  $-\frac{1}{2} < \lambda_i - \gamma_i < \frac{1}{2}$  where  $\gamma_i$  is a five component parameter which is the displacement of  $R^2$  a plane which intersects the 5D lattice. If  $\sum_i \gamma_i = \frac{1}{2} \pmod{1}$  a Penrose pattern is formed with 5 fold symmetry [28] [26] [12].

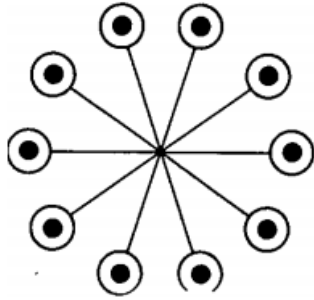


Figure 13: Ten point unit cell. Adapted from reference [12] figure 6.

Software to perform these steps was written by my supervisor Gavin Burnell before this project had started. My starting point was computer object which included all the Penrose vertices and their adjacent neighbours. Each tiled unit cell consisted of a ten point star (see figure 13). Each leg of the star was either populated or not depending on the class of vertex and its orientation. Each vertex class is classified with a code which relates to a ten bit binary digit which arises from whether each leg is populated or not. Each vertex is rotated such that each ten bit number is the lowest number possible.

### **Limiting case MC**

For the Penrose geometry system one technique available is the limiting case Monte Carlo. Part of the distribution is set to the skeleton mask. All other points in the system which are not a member of the mask will be allowed to evolve freely. The subset of states which do not depend on the mask will be examined for properties such as long range order. The interactions of the flip islands will be investigated for their energy contribution to the system. The technique potentially could determine a ground state for the rest of the system excluded by the mask as the effects of geometrical frustration will be negated. Interactions of flippable dipoles with static members of the mask were explicitly calculated.

### **0.2.5 Software**

The Enthought distribution of python has been used to write the relevant software for this project. The Enthought distribution contains many useful packages to aid in scientific endeavours. Enthought includes Numpy a package for dealing with arrays, SciPi which includes functions to evaluate statistics and finally MatPlotLib for compiling graphs. GUI software elements were made with Tkinter.

A large amount of time in this project was devoted to creating the required software to perform simulations and to analyse the resulting data. A great effort was made in creating a real-time monitor which handled multiple simulations simultaneously, via networking techniques. MC runs could be run on multiple independent computers concurrently. The amount of time devoted to generating the software limited the amount of available time for simulations and analysis. Having a robust and adaptable program was imperative for conducting research of this type, therefore spending a large amount of time developing it was justified.

Careful consideration of all aspect of the program led to a highly efficient algorithm which was capable of simulating large systems of up to 1650 dipoles in a reasonable amount of time.

Several issues technical issue were encountered. Making computers with different operating systems to communicate in a consistent manor proved troublesome but these problems were overcome with time.

### **0.2.6 Statistical analysis**

Configurational entropy is the entropy due to the arrangement of the component parts of a system rather than disordered arising from momentum or velocity. Boltzmann's entropy formula relates the entropy( $S$ ) to the number of possible configurations( $\Omega$ ):  $S = k_B \ln(\Omega)$ .

MC simulations of spin ice will, as indicated previously, generate ensemble averages at a fixed temperature. Statical techniques can then be used to estimate some physical properties of the system at each stage.

Calculating properties via the variance of quantities is known as the fluctuation dissipation theorem, it is a very powerful tool in statistical physics for describing non-equilibrium dynamics [13]. The variance of the energy can be used to determine the heat capacity of a system (the derivation is available in the appendix).

$$C_v = \frac{\beta}{T} (\langle E^2 \rangle - \langle E \rangle^2)$$

An equivalent is available employing the variance of the magnetisation to predict the magnetic susceptibility of a material.

$$\chi = \beta (\langle M^2 \rangle - \langle M \rangle^2)$$

In science it is always important to quantify the certainty in which properties are known. There are two techniques available for generating errors for quantities arising from the variance of a sample variable.

One technique in quantifying the error is to compare a set of simulations which experienced the same temperature decent, but which had independent initial conditions. The heat capacity and susceptibility can be averaged over the different runs and errors obtained. This technique requires having a sufficiently large number of parallel runs from which to compare. At least three simulations in a group are required to generate any meaningful statistics.

In the case where insufficient equivalent data is available there exists another technique which can help. Statistical bootstrapping is a method for assigning measures of accuracy to a computed statistic from a sample distribution. The technique is quite simple and allows the appointment of errors without prior knowledge of the parent distribution from which samples are drawn.

The procedure is as follows; the super-sample is obtained from an ensemble with fixed temperature, call this super-sample frame  $M$ .  $N$  frames are chosen at random from Frame  $M$ ,  $b$  times such that  $M > bN$ . Statistical averages and errors are then calculated from the  $b$  sets of  $N$  frames [4].

### 0.2.7 Square ice test case

Results for the square spin ice test case are presented. Firstly one will present the classification of the vertex types and the calculation of the configurational entropy. Next the energy change landscape is presented and the effective energy determined. Subsequently the simulation data and statistical analysis conferred before conclusions are drawn.

#### Square vertices and entropy

The square lattice can be decomposed into a square unit cell called a vertex. Each vertex can be arranged in sixteen different ways and organised into four groups with the same energy. The configurational entropy of each vertex is as follows:

$$S = k_B \ln(\Omega) = k_B \ln(16) = 3.622 \times 10^{-23} [J/K]$$

The system to be simulated has 264 dipoles each with 2 configurations, thus the total entropy is:  $S = k_B \ln(\Omega) = k_B \ln(2^{264}) = 2.526 \times 10^{-21} [J/K]$

Vertex type	1	2	3	4
Configuration				
Energy [J]:	1.53e-19	0	2.04e-20	-1.93e-19
Degeneracy:	2	8	4	2
Probability:	0.125	0.5	0.25	0.125

Figure 14: The different unique vertex topologies available to the system, organised in terms of energy, type 1 has the highest energy and 4 the lowest. The probability associated with the degeneracy indicates what the distribution of vertex populations should converge to at high temperature.

#### Energy landscape

An energy change landscape was computed for 1000 MC steps for a total of 264,000 spin flips.

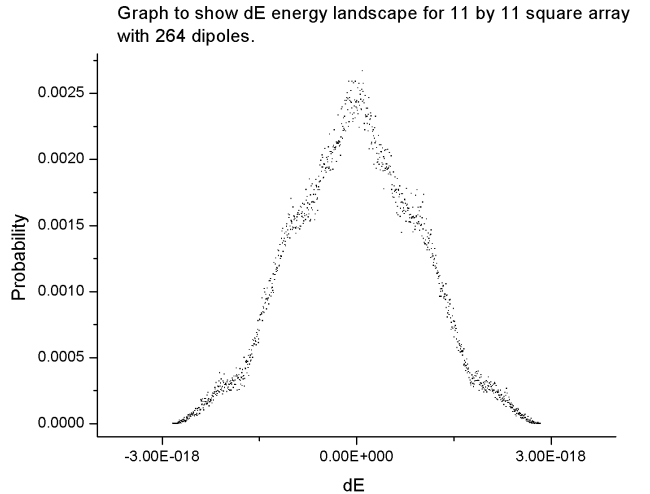


Figure 15: From this diagram an energy scale of  $1.312 \times 10^{-18} [J]$  was determined. The distribution deviates only slightly from a true normal curve.

#### Simulation

Two concerted simulations (run 1 and 2) form this group. Each run simulates an  $11^2$  square array of vertices with over 10,000 MC steps and a range of 11 different  $\alpha$ 's starting from  $\alpha = 1000$  (a large temperature to ensure each system is well distributed according to the degeneracy) to  $\alpha = 0.0625$ . The number of MC steps per fixed  $\alpha$  varies due to the requirement of vertex population satisfaction, but full details are available in the appendix tables 4 and 5.

As only two simulations are available for comparison, not enough equivalent data is available for errors arising from the combination of simulation data sets. Statistical bootstrapping was used to generate errors for the heat capacity and magnetic susceptibility (see

appendix for details). Vertex populations and magnetisation order parameter averages and errors were calculated from the sample statistics available within each stage.

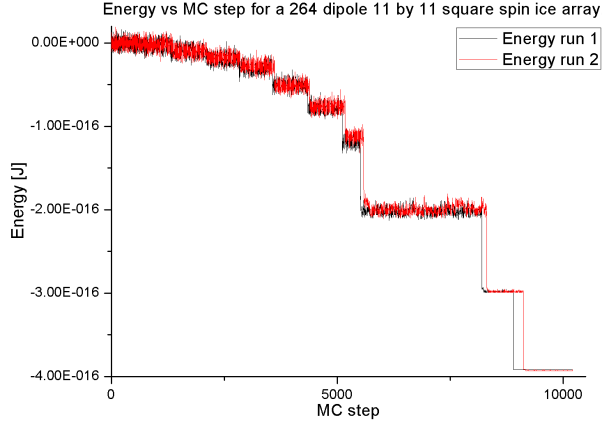


Figure 16: Energy decent for this simulation resulting in a lowest energy of nearly  $-4e-16[J]$

## Analysis

Deviation from the high temperature distribution starts at around  $\alpha = 1$ . As  $\alpha$  is subsequently lowered the population in the ground state (vertex type 4) approaches unity and the other vertex populations drop to zero.

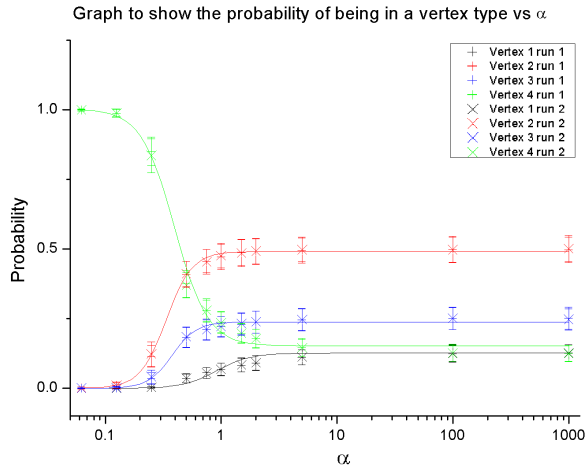


Figure 17: As  $\alpha$  is lowered the populations indicate energy minimisation and the simulated ASI enters the ground state. Initially ( $\alpha = 1000$ ) the vertices are well distributed according to the high temperature populations as depicted in figure 3, although the best fit logistic function does not depict this well, if one observes the data points it is evident.

Figure 17 is reminiscent of figure 5 although the parameter on the x-axis is an inverse temperature coefficient in figure 5 and thus the axis is reversed. Demian Levis in his paper 'Thermal phase transitions in Artificial Spin-Ice' [15] did not fix a value for the magnitude of the magnetic moment, instead his data is normalised in terms of the ratio of Boltzmann weights. The data is not easily comparable to my own without reweighing all the values which due to time constraints this was not possible.

To compare the heat capacity of the system it is important to calculate a ball park figure. One can derive an estimate for the heat capacity a permalloy sample with the same volume of the system. The density of permalloy is taken to be  $8720[kgm^{-3}]$  [1], the heat capacity at room temperature is  $4.6 \times 10^{-4}[Jkg^{-1}K^{-1}]$  [?], and finally the volume of each island is  $5.46 \times 10^{-22}[m^{-3}]$  yielding a heat capacity per island of  $2.19 \times 10^{-21}[JK^{-1}]$ .

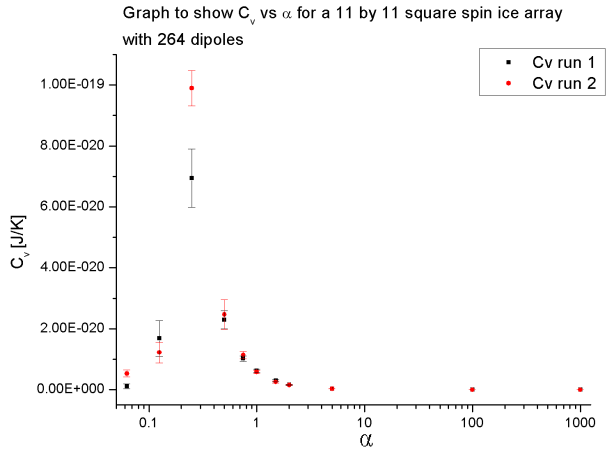


Figure 20: The heat capacity showing a distinctive peak at  $\alpha = 0.25$

The heat capacity which is derived from the variance of the energy at fixed temperature shows a distinctive peak at  $\alpha = 0.25$  which is evidence of a critical temperature of  $23,768[K]$ . Clearly this temperature is far too high to be physical. One explanation for such a high temperature is the incorrect assumption of total saturation of the magnetic islands. The energy of an interaction is proportional to the square of the magnetisation saturation. If for instance one assumes that the magnetisation is only 10% saturated then the energy will need a correction factor of 0.01 and thus the critical temperature will in this case be  $237.68[K]$  which seems more plausible. For the simulated square system of 264 dipoles an estimate for the heat capacity is  $5.8 \times 10^{-19}[JK^{-1}]$ , which is a higher than the peak heat capacity achieved by run 2 at  $1 \times 10^{-19}[JK^{-1}]$  but is in a range which seems somewhat sensible. The heat capacity arises from

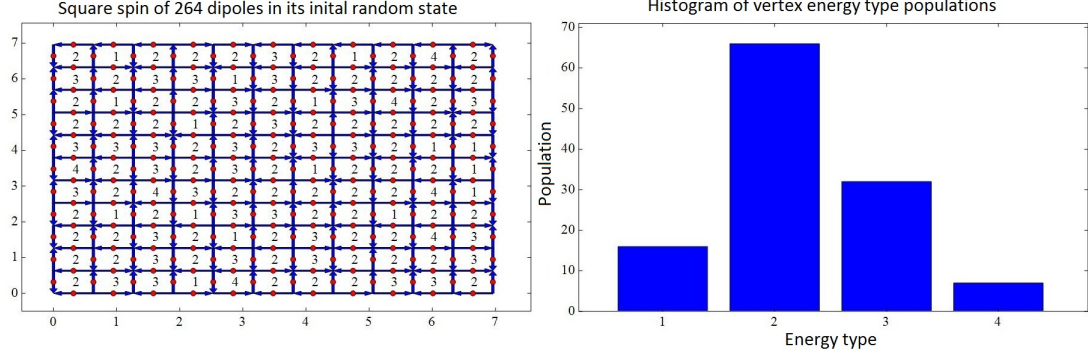


Figure 18: Distribution (left) and vertex population histogram (right) of a square spin ice state in its initial state with randomised polarities. Note that the initial state does not exactly match the high temperature configuration, as the system is thermalised at  $\alpha = 1000$  the vertex populations do indeed converge on the infinite temperature distribution.

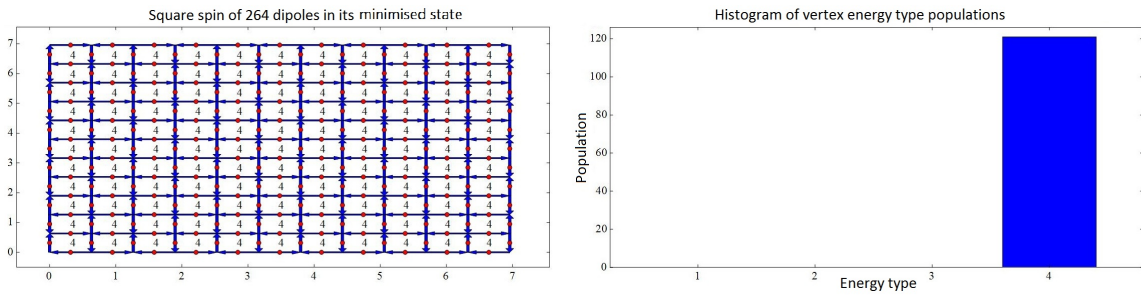


Figure 19: Distribution (left) and vertex population histogram (right) of a square spin ice state in its final minimised configuration at MC step 10183. All vertices are in energy configuration type 4 which is the lowest energy. The system is in the antiferromagnetic ground state.

the variance of energy, the variance of the energy is the average of the squared difference from the mean. The heat capacity value calculate is dependant on the magnitude of the energy, and thus if the energy is wrong by a constant factor this will skew the heat capacity.

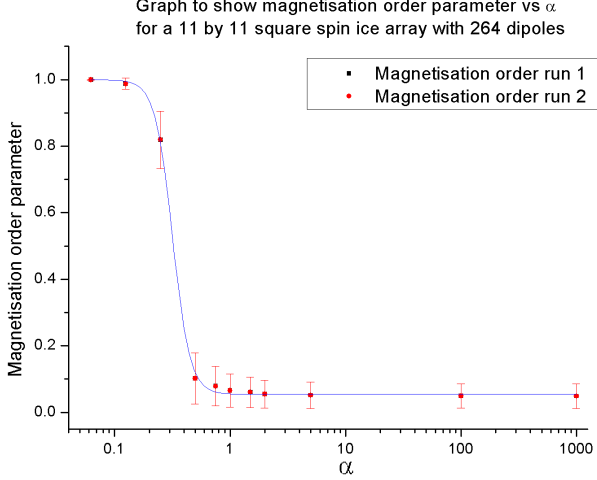


Figure 21: The magnetisation order parameter approaches unity over the course of the simulation. Run 1 data appears to be absent however it is in fact just obscured by the second runs data.

As expected the magnetisation parameter indicates that at low temperature  $\alpha = 0.0625$  the system is in its ground state the error on the last points is very small showing that at this temperature the state is effectively frozen.  $\alpha = 0.0625$  corresponds to  $6180[K]$  or  $61.80[K]$  with 10% saturation. Figure 21 is similar to figure 6 although as the modifiable parameter Demian Levis used is the inverse temperature, thus the axis are reversed.

The magnetic susceptibility shows a peak at  $\alpha = 0.25$  in agreement with the peak in the heat capacity. Data from run 1 appears to be absent however this is due to the points and errors being so similar that they in fact super impose on another. I was unable to find a value of the susceptibility of permalloy in the literature and therefore unfortunately it was not possible to make a comparison.

## Conclusion

It was possible to achieve the ground state distribution over a reasonable number of steps. Estimation of the critical temperature proved difficult as the degree of magnetisation saturation is unknown. The calculated heat capacity does seems plausible however it is affected by the saturation issue. The magnetic susceptibility without comparable data is not much use but for confirming the critical temperature.

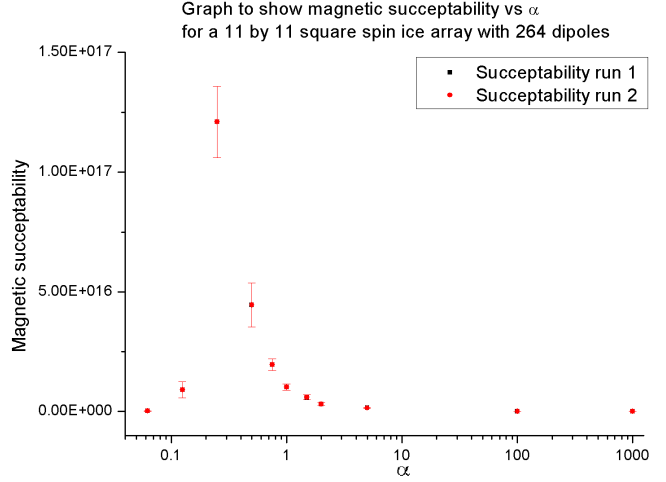


Figure 22: The calculate magnetic susceptibility of the system showing a clear peak at  $\alpha = 0.25$

## 0.3 Monte Carlo simulation and statistical analysis of Penrose ASIs

Results for the 720 and 1650 dipole Penrose spin ice are presented. Firstly one will present the vertex classification and entropy calculations. Next the 720 dipole system will be discussed, its energy landscape depicted and analysed. Subsequently the details of the simulation group outlined before the statistical analysis of the heat capacity and vertex populations. Similarly for the 1650 dipole system, the energy landscape will be investigated before moving on to analysis which included the heat capacity calculations, the vertex populations, the partial magnetisation order parameter and estimates for the partial magnetic susceptibility. In the final section one will explore the result of the limiting case MC.

### 0.3.1 Vertex classification and entropy

The Penrose spin ice can be decomposed into seven units (known as vertex classes) cells which are tiled to form the pattern, their neighbouring vertex classes are unique spatially. Each vertex class(VC) has a set of unique energy configurations known as energy types(ET). For convenience the energy types have been organised, the lower the energy type number the lower the energy, such that an energy type of one is the ground state for that vertex class.

The entropy of each vertex class can be calculated from the total number of configurations available for each class the result are depicted in table 1 (see table 10 and 11 in the appendix for further details.)

Total entropy of each system can be calculated by considering the binary configurations of each of

Table 1: Entropy calculations for each vertex class

Vertex class	Total configurations	Entropy [J/K]
1	8	$2.87098 \times 10^{-23}$
2	8	$2.87098 \times 10^{-23}$
3	16	$3.82797 \times 10^{-23}$
4	32	$4.78496 \times 10^{-23}$
5	32	$4.78496 \times 10^{-23}$
6	64	$5.74196 \times 10^{-23}$
7	128	$6.69895 \times 10^{-23}$

the constituent dipoles. The total entropy of the 720 dipole system follows:  $S = k_B \ln(2^{720}) = 720k_B \ln(2) = 6.89 \times 10^{-21} [J/K]$  The total entropy of the 1650 dipole system is:  $S = k_B \ln(2^{1650}) = 1650k_B \ln(2) = 1.58 \times 10^{-20} [J/K]$

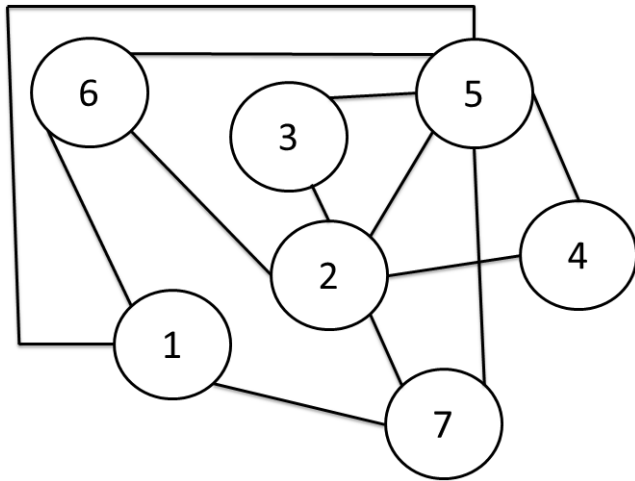


Figure 23: A mathematical graph was obtained for the Penrose system, symbolising how each vertex class connects to adjacent vertex nodes. The graph is irreducible.

Figure 24 yields some evidence that a ground state for the system will most likely involve vertex class 2 and 7 with some or all population in the first excited state. The energy gap indicates that having excited populations in these vertex classes will minimally impact upon the energy. As the energy gap is much greater for the other classes it is most likely that these will be in the ground state for a global energy minimum.

In the limiting case MC, the skeleton mask implies vertex classes 4 and 6 are free to vary. By analysing the connectivity graph (figure 23) one can infer that classes 1,2 and 5 are connected to the flipable vertices. Classes 1 and 5 however have degenerate dipoles in their ground state (see figure 24) which connect directly to the flipable vertices, therefore these classes will not experience any population changes during the limiting case MC. Only classes 2,4

and 6 are effected.

### 0.3.2 720 dipole system

Simulating large Ising systems with Monte Carlo is time intensive. To get an idea of the system dynamics, a system with 720 dipoles will be simulated before moving on to the 1650 dipoles system.

#### Energy landscape

An energy landscape was generated with 1000 MC steps for a total of 720,000 spin flips.

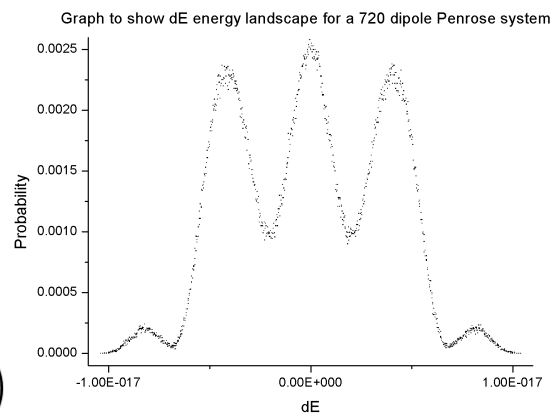


Figure 25: The distribution is deviates significantly from a normal distribution. Energy scale was calculate using the method identified before yielding a value of  $5.456 \times 10^{-18} [J]$

The energy landscape in figure 25 seems quite dissimilar from the square spin ice landscape. The landscape is much broader than the one calculated for the square system. The figure features many distinct stationary points.

#### Simulation

Two concurrent simulations (run 1 and 2) with a length of over 30000 MC steps were performed over a range of 22 different  $\alpha$ 's starting from  $\alpha = 1000$  to  $\alpha = 0.005$  details in the appendix (tables 6 and 7).

Only two simulations are available for comparison. Insufficient equivalent data is available to calculate averages and errors from the combination of the simulation data sets. Instead statistical bootstrapping was used to generate errors for the heat capacity. Vertex population averages and errors were calculated from the ensemble data set available within each run. The ground state skeleton mask, due to time constraints was not implemented for this system size. The partial order parameter and magnetic susceptibility calculations are not therefore available.

Vertex class	1: Code 69	2: Code 73	3: Code 85	4: Code 341	5: Code 155	6: Code 343	7: Code 375
Ground state							
First excited state							
Normalised energy gap	9.138	1.886	9.138	18.27	3.479	15.94	1.000

Figure 24: Ground and first excited states of the seven vertex classes. The energy gap between the ground and first excited state of vertex class 2 and 7 are the lowest.

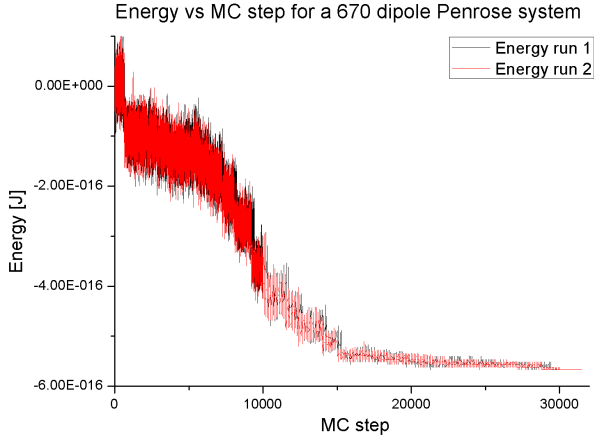


Figure 26: Energy decent over the course of the simulation. The system falls much lower than  $-4 \times 10^{-16} [J]$  which was not quite reached by the 264 dipole square system, this is expected as the Penrose system is larger and thus in a low energy configuration there are more vertices available to contribute negatively to the global energy.

### Analysis

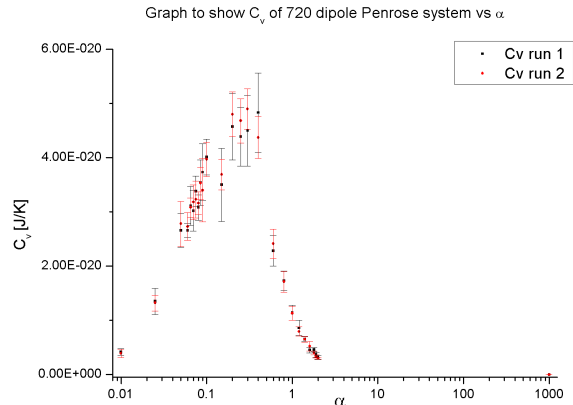


Figure 29: The heat capacity of the 720 dipole Penrose system which peaks at around  $\alpha = 0.3$

Using the previously derived heat capacity per island one can estimate the heat capacity of permalloy with an equal volume to this system. I estimate the heat capacity to be  $1.577 \times 10^{-18} [JK^{-1}]$  compared to the maximum peak of around  $4.9 \times 10^{-20} [J/K]$  the calculated heat capacity is around two orders of magnitude lower.

The peak of the heat capacity which is indicative of approaching a critical point. The peak occurs at  $\alpha = 0.3$ , corresponding to a temperature of

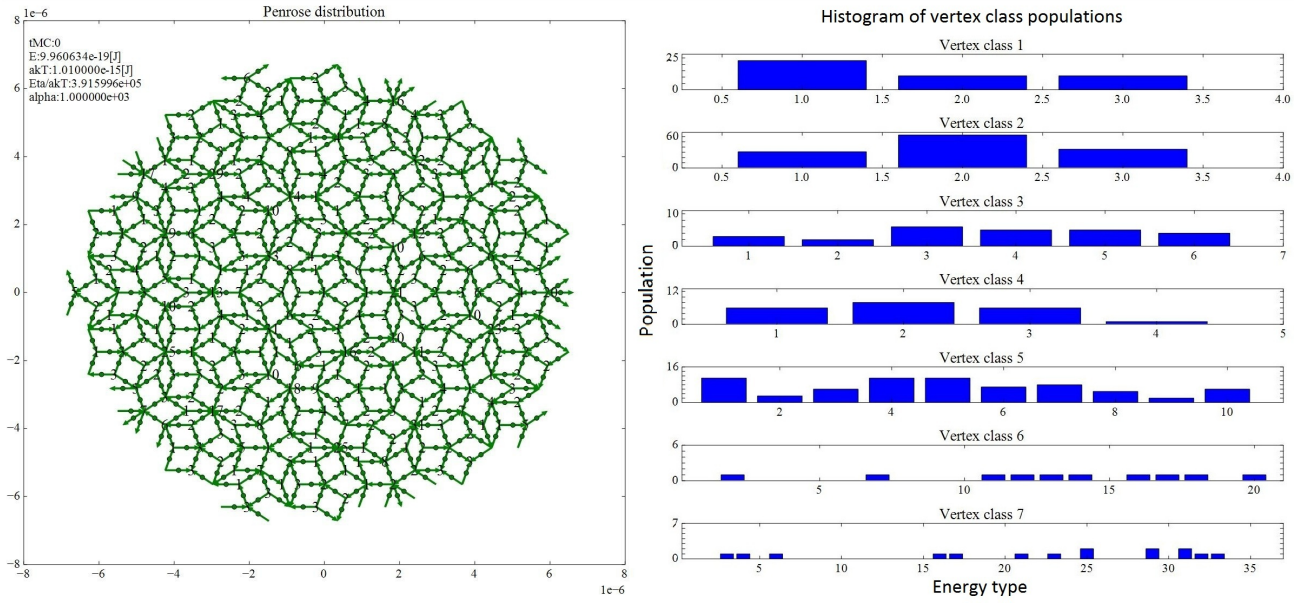


Figure 27: Distribution (left) and vertex population histogram (right) of a Penrose state (run 2) with 720 dipoles in its initial randomised configuration. The energy of this state is  $5.38 \times 10^{-18} [J]$

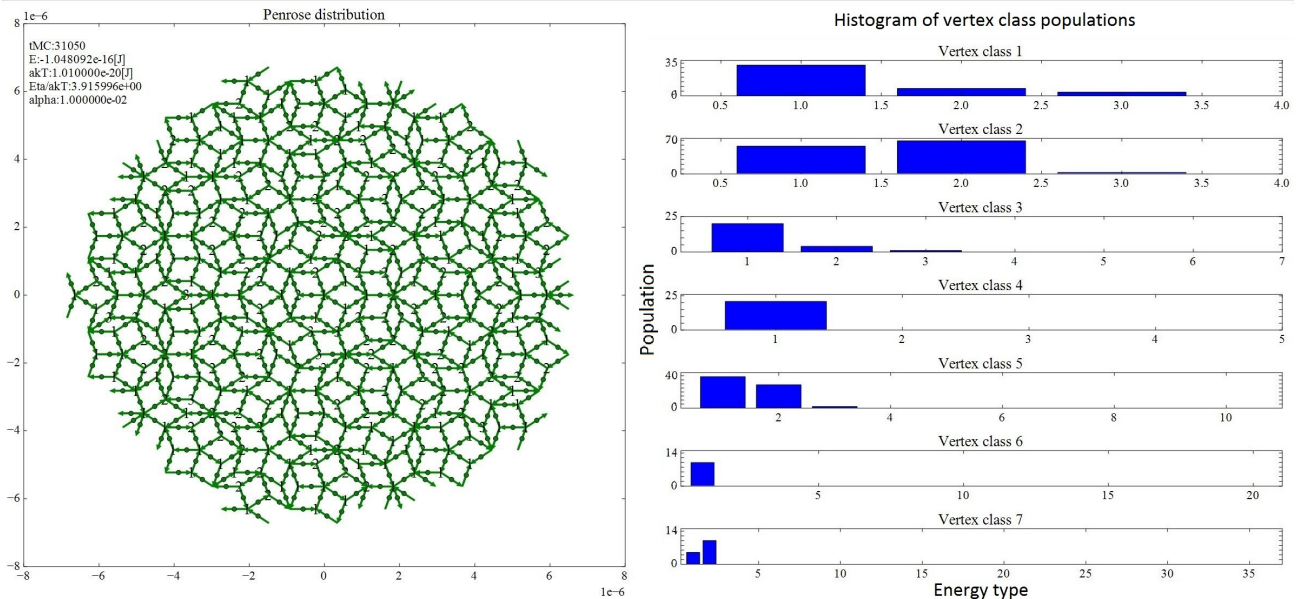
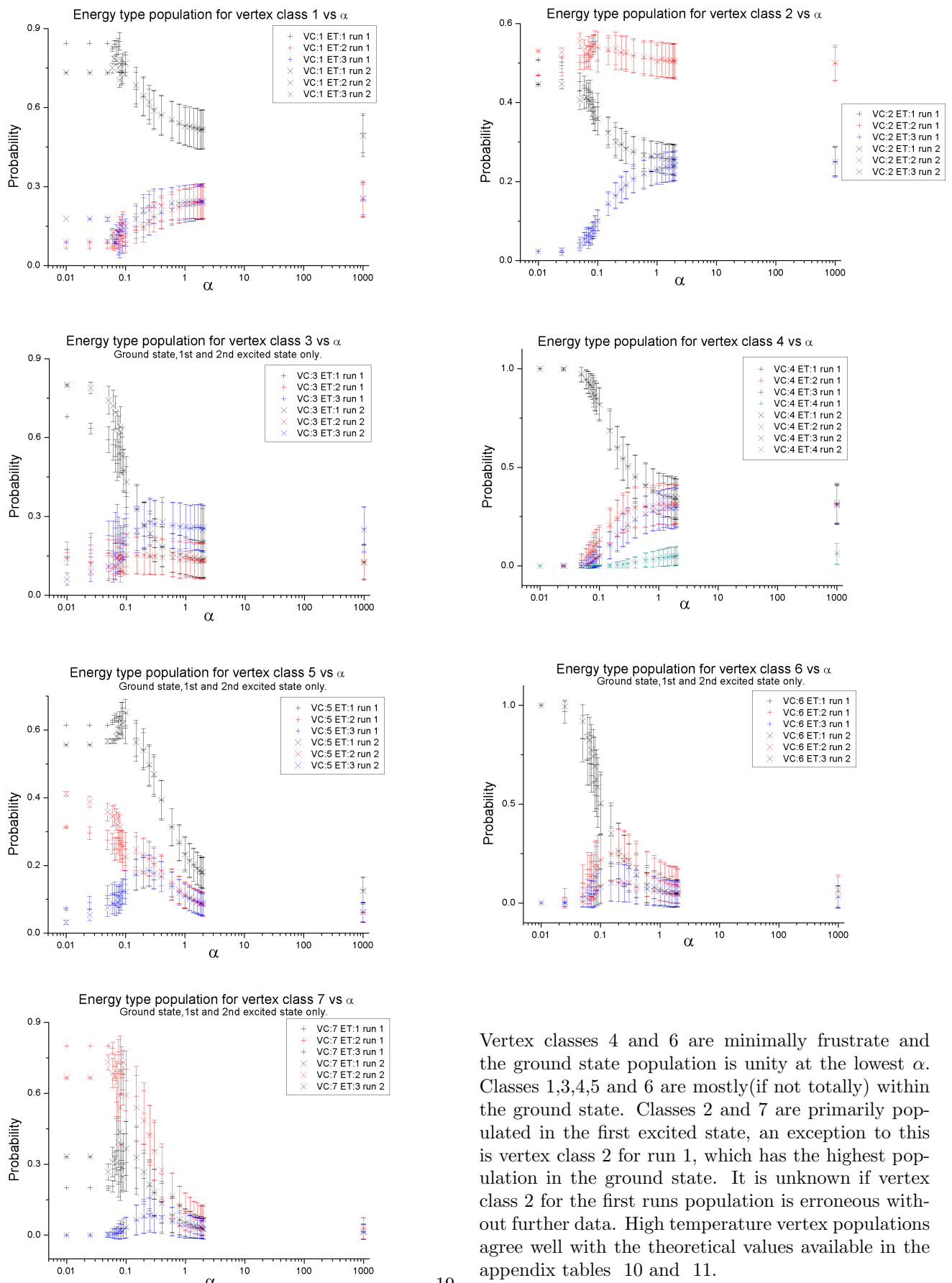


Figure 28: Distribution (left) and vertex population histogram (right) of a Penrose state (run 2) with 720 dipoles after 31050 MC steps. Classes 1,3,4,5 and 6 have a majority population in the ground state whereas classes 2 and 7 are predominantly populated in the first excited state. The energy of this state is  $-5.66 \times 10^{-16} [J]$

$118,696[K]$  assuming saturation, or  $1187[K]$  assuming 10% saturation. Certainly the lower limit seems more sensible.

Table 2:  
Vertex class populations for 720 dipole Penrose system



Vertex classes 4 and 6 are minimally frustrate and the ground state population is unity at the lowest  $\alpha$ . Classes 1,3,4,5 and 6 are mostly(if not totally) within the ground state. Classes 2 and 7 are primarily populated in the first excited state, an exception to this is vertex class 2 for run 1, which has the highest population in the ground state. It is unknown if vertex class 2 for the first runs population is erroneous without further data. High temperature vertex populations agree well with the theoretical values available in the appendix tables 10 and 11.

## Conclusion

There is not enough evidence to conclude that the vertex populations of classes 2 and 7 prefer the first excited state for a global minimum. It is quite evident due to non zero populations in energy type 3, that the global minimum was not achieved in over 30000 steps. Indicating just how difficult minimisation of geometrically and magnetically frustrated systems can be. Assuming the magnetic islands are totally saturated, has resulting in un-physical transition temperatures for both this system and the square system alike. Heat capacity calculations are affected. Without some direction from experiments as to the totality of saturation, it is unlikely this problem will be resolved.

### 0.3.3 1650 dipole system

Experimental data exists for the 1650 dipole Penrose ASI. One initially wished to compare a range of lattice parameters over a range of  $700\text{nm} \rightarrow 1000\text{nm}$  at room temperature. Regrettably an error in calculating the the volume of a nano-island was made and thus the  $\alpha$  values which corresponded to these lattice parameters were skewed by a constant. The volume error was corrected for in each simulation set but comparison to experiment was therefore not possible. Moreover I had wished to measure how the system freezes as a function of the islands thickness, however with the true dipole moment unknown, this is difficult to quantify in real terms.

The skeleton mask was implemented for this system, partial magnetisation order parameters and the partial susceptibility have been calculated.

Three concurrent simulations data are available, the data sets were combined to determine averages errors for the heat capacity and magnetic susceptibility. Vertex population and magnetisation order parameter errors were calculated from within their own respective ensemble data sets.

## Energy landscape

An energy landscape was generate with 1000 MC steps for a total of 1,650,000 spin flips.

The effective energy for this system is slightly higher than the calculation for the previous 720 dipole Penrose spin ice. The distribution does seem to have a similar width( $\approx 1 \times 10^{-17}[\text{J}]$ ) when compared to the last evaluated energy landscape. As the width of the energy landscape has not changed, one can infer there is not a strong dependence of the transitional energies compared with the system size.

The stationary points 1,2,3,4 and 5 have an associate  $\alpha$  of 0.34924, 0.72233, 1.2118, 1.4599 and 1.8416 respectively.

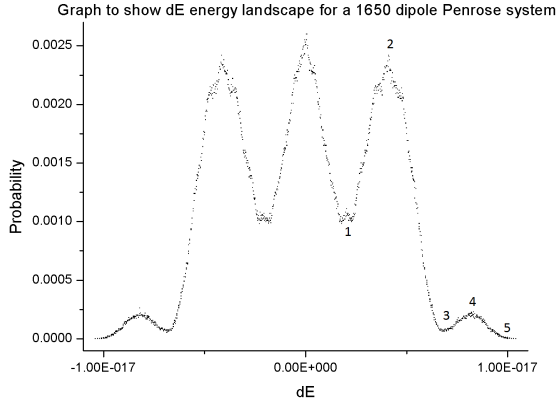


Figure 30: The distribution again deviates significantly from a normal distribution. The landscape has multiple stationary points. Note that the peaks are now perturbation. Stationary points have been labelled. Energy scale was calculate using the method identified with a value of  $5.661 \times 10^{-18}[\text{J}]$

## Simulation

The three simulations(run 1,2 and 3) were performed over a range of sixteen  $\alpha$ 's in over 12,000 MC steps (details in appendix table 8). The system dynamical evolved until around MC step 8000 before the spins settled (but did not freeze), the rest of the simulation did not make a significant contribution to energy minimisation. In hindsight too little time was spent in the region with large population fluctuations(the transition region), the system was cooled to aggressively and not enough time was spent equilibrating the system at each stage.

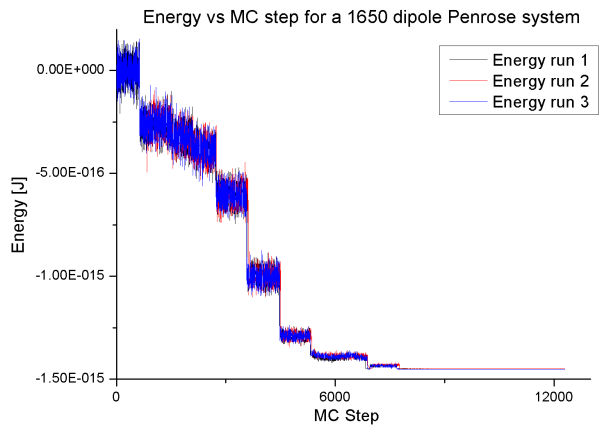


Figure 31: The energy decent of a 1650 dipole system.

Less data was available in the transition region than for the 670 dipole Penrose simulation. The statistics

may have inferior quality than before. Moreover as this system is larger and the number of interaction calculations more numerous, there are fewer MC steps than the last simulation set (see appendix table 8.)

## Analysis

The issue associated with the saturation affect is still significant for this data. As such it is hard to draw a definitive conclusion about the heat capacity. One can however comment on the data relative to the previous simulation.

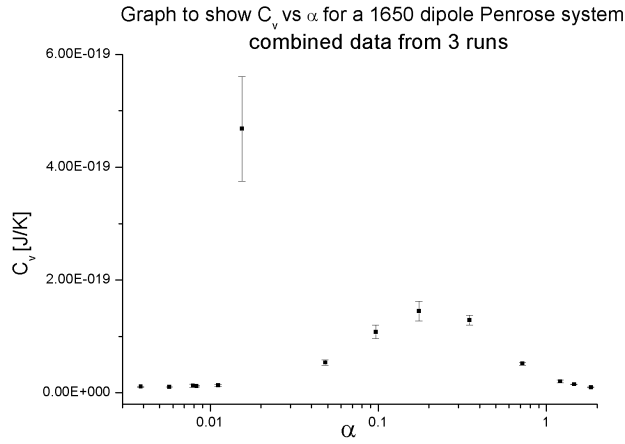


Figure 34: The heat capacity of the 1650 dipole Penrose system, it show two peaks at  $\alpha = 0.17462$  and another at  $\alpha = 0.015448$

The two peaks at  $\alpha = 0.17462$  and  $\alpha = 0.015448$  assuming total saturation correspond to a temperature of  $71,632[K]$  and  $6333.8[K]$  respectively or assuming 10% saturation  $716.32[K]$  and  $63.338[K]$ . Both of these sets of critical temperatures are lower than the 670 dipole equivalent.

It is possible that the large transition from  $\alpha = 0.048275$  to  $\alpha = 0.015448$  affected the heat capacity calculation for the data point where  $\alpha = 0.015448$ . Without more data it is uncertain if the peak at  $\alpha = 0.015448$  is a true peak or an artefact, not enough data either side of this value is available to extrapolate a trend. The other lower peak on the other hand has the surrounding points to support it as being a valid peak.

The lower peak in the heat capacity occurs at  $(1.45 \pm 0.2) \times 10^{-19}[J/K]$  and the higher peak has a heat capacity of  $(4.68 \pm 0.9) \times 10^{-19}[J/K]$ . Using methods identified before an estimate for the heat capacity of an equivalent volume of permalloy is  $3.6137 \times 10^{-18}[J/K]$ . Both heat capacity peaks are lower than the ball park figure. The larger peak is around an order of magnitude higher than the heat

capacity of the 720 dipole peak, the lower peak is about 3 times higher.

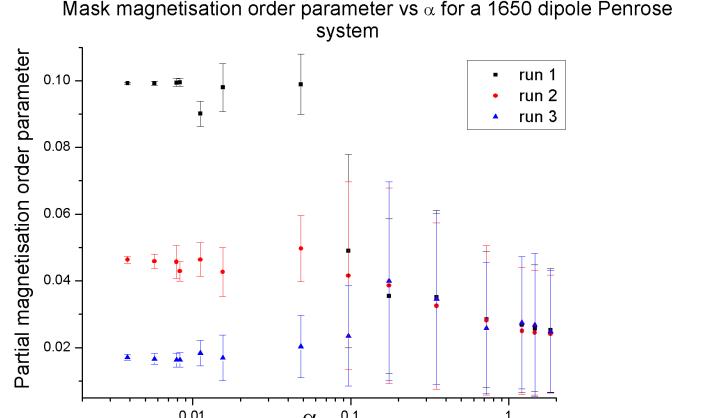


Figure 35: The partial mask magnetisation order parameter for 3 runs, there is a large discrepancy between the runs in their final states. At large  $\alpha$  the error bars for the magnetisation order parameter are large this is to be expected as the system is in a spin-liquid like state and the order is free to fluctuate. At low  $\alpha$  the error bars are small but non-zero indicating that the system has not entirely frozen and some dynamic behaviour still occurs.

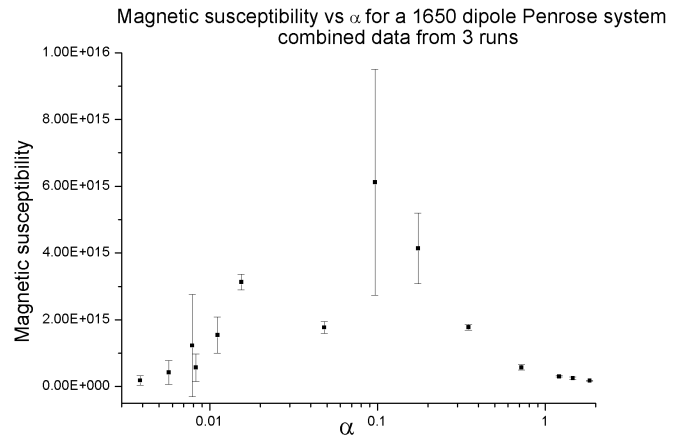


Figure 36: The partial magnetic susceptibility, this graph does not show a clear peak the largest value is obtained at  $\alpha = 0.09655$  however it also has the largest error.

The quality of the statistic gathered for partial magnetic susceptibility depicted in figure 36 is insufficient to draw conclusions and data for comparison is not available.

It is not certain as to what this susceptibility even

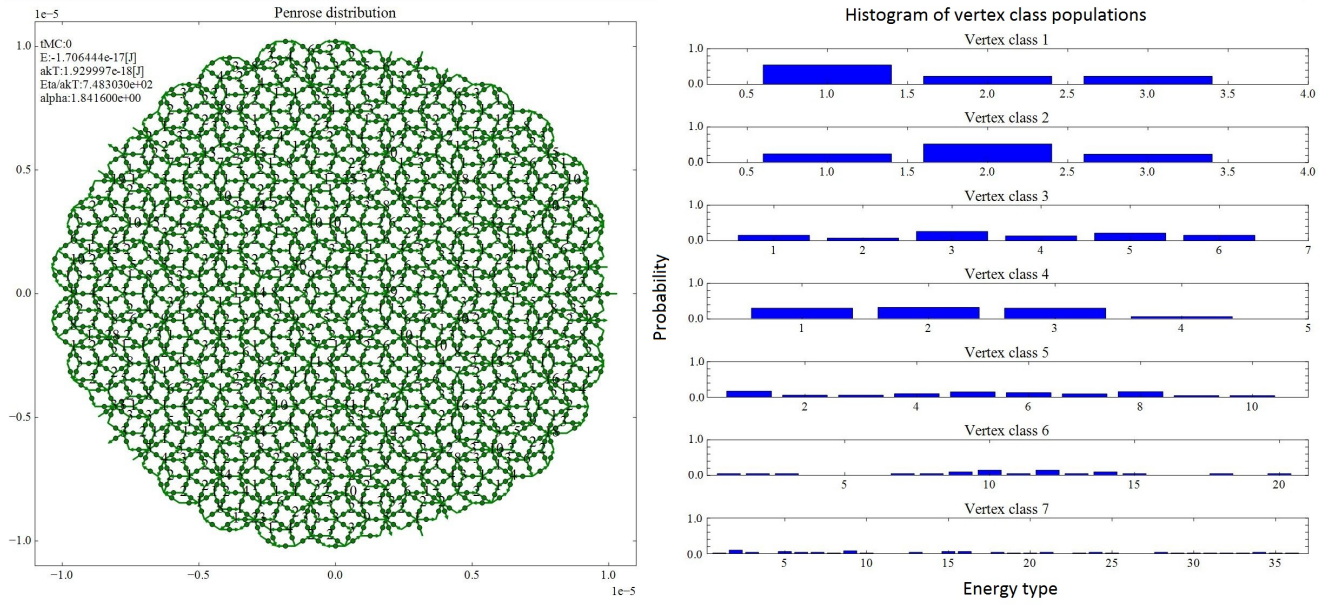


Figure 32: Distribution (left) and vertex population histogram (right) of a Penrose state with 1650 dipoles in its initial state with randomised polarities. The energy of this state is  $-9.21765 \times 10^{-17} [J]$ .

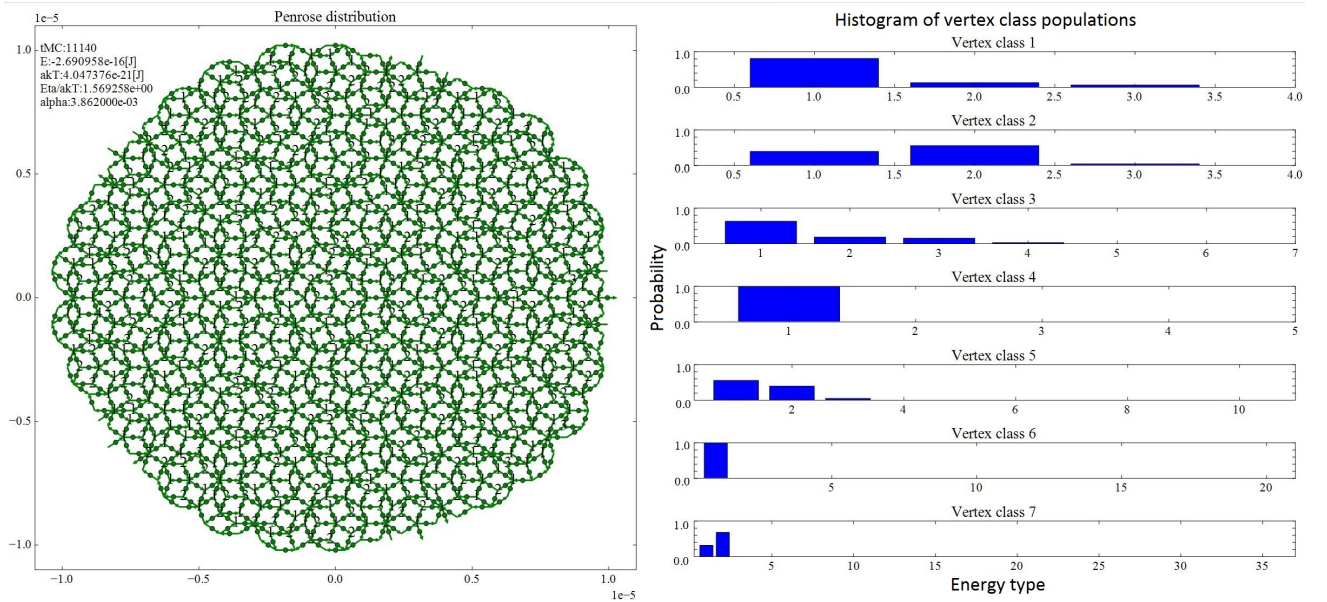
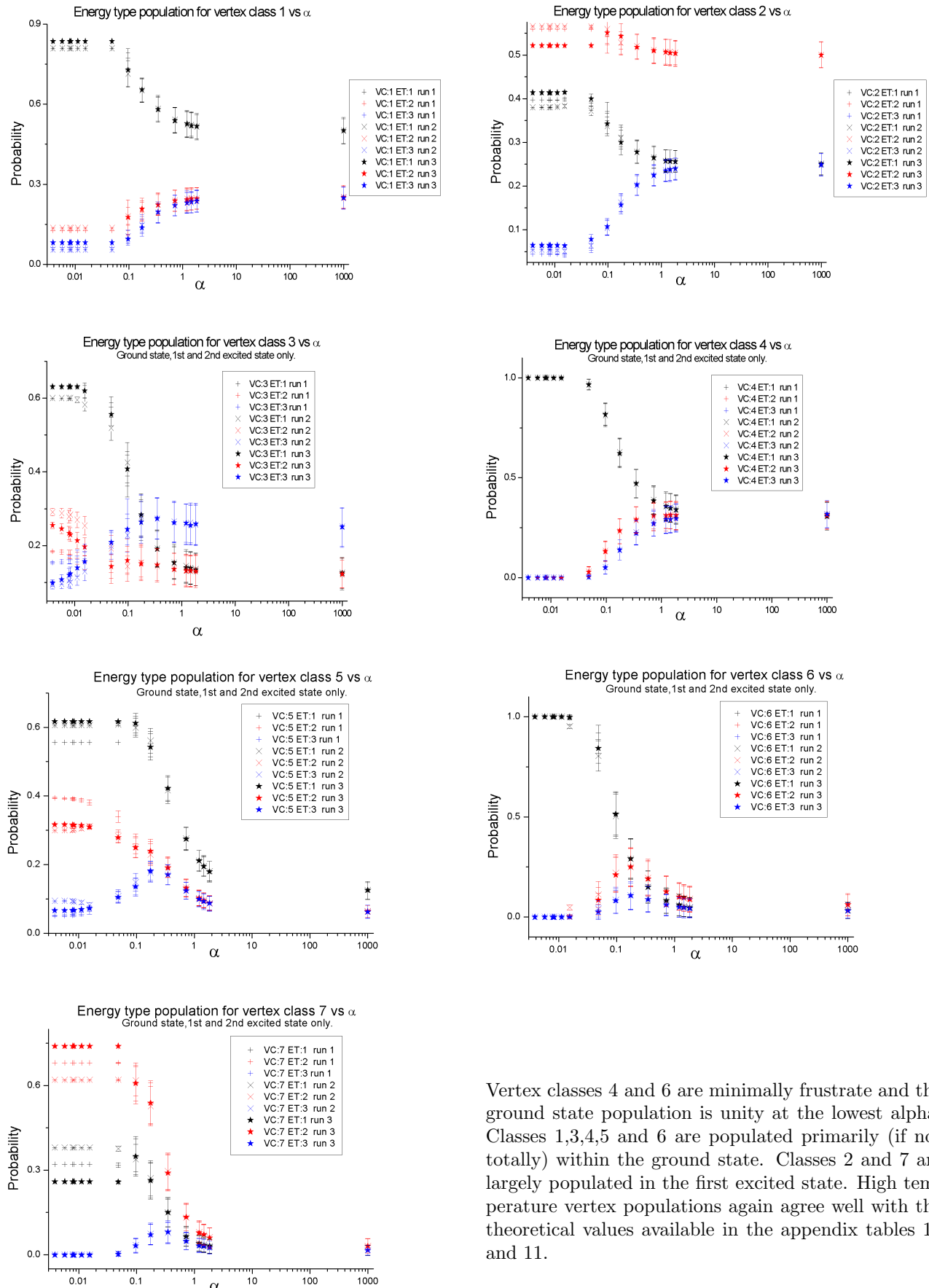


Figure 33: Distribution (left) and vertex population histogram (right) of a Penrose state with 1650 dipoles after 11,140 MC steps. Vertex class 4 has some population in energy type 4, which was negligible in the 720 dipole simulation, perhaps indicating that the system is well minimised. The energy of this state is  $-1.453567 \times 10^{-15} [J]$ .

means in the context of a real physical parameter. The susceptibility is a dimensionless constant which relates the magnetisation to a parallel field. A Penrose pattern is five fold symmetric. If one could define a 2D field which was parallel to some section of the dipoles, then the field would not be parallel to the remaining dipoles.

In 5D one could conceive of a field which would be parallel to each vertex in the 5D cubic lattice. However this field is hypothetical with no real counterpart in 2D.

Table 3:  
Vertex class populations for 1650 dipole Penrose system



Vertex classes 4 and 6 are minimally frustrate and the ground state population is unity at the lowest alpha. Classes 1,3,4,5 and 6 are populated primarily (if not totally) within the ground state. Classes 2 and 7 are largely populated in the first excited state. High temperature vertex populations again agree well with the theoretical values available in the appendix tables 10 and 11.

## Conclusion

Vertex data in table 3 is further evidence that vertex classes 2 and 7 do seem to prefer a majority population in the first excited state and that the other vertex classes settle to have most of their population in the ground state. The persistent issue of the saturation has made it extremely difficult to draw conclusions concerning the heat capacity. Equivalent data in the literature is unavailable for comparison.

### 0.3.4 Limiting case MC

The difficulty in extracting real world properties from the simulated data has somewhat limited the scope of this project. One method is left to explore the lower energy state of the system by exploring the dynamics outside of the skeleton mask, with the ambition of testing whether or not the flip island configuration relative to one another affect the energy of the system.

As the skeleton mask is fixed, there was no point calculating the partial magnetisation order parameter. This limiting case MC of the 1650 dipole system represents a totally artificial system. It would be difficult to make a real ASI, where some dipoles were fixed and other free to flip, although not impossible. As this simulation is not testable against a physical experiment I did not concern myself with finding the heat capacity. Without needing to find the heat capacity, long periods of time did not need to be devoted to equilibrating the system and instead a large range of  $\alpha$ 's were explored.

## Simulation

Two concurrent simulations(run 1 and 2) were performed over a range of 23 different  $\alpha$ 's in just over 3500 MC steps (see appendix table 9 for details.)

The limiting case MC simulation did succeed in generating a lower energy than the non-limiting case. With the effects of frustration negated, minimising the system was more successful.

## Analysis

Vertex class populations 1,3,5 and 7 were fixed by setting the skeleton mask. Vertex classes 1,3 and 5 are found in the ground state with populations 110, 65 and 180 respectively. Vertex class 7 is in the 1st excited state with population 50. The remaining three vertices 2,4 and 6 vary over the course of the simulation.

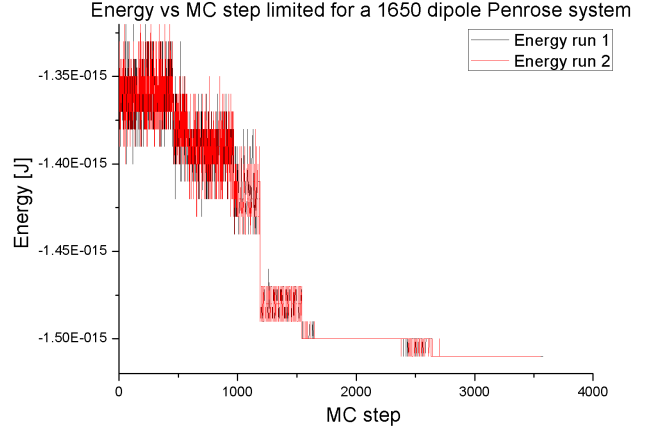


Figure 37: Energy decent of the limited case Monte Carlo simulation. The final energy  $\approx -1.51 \times 10^{-15} [J]$  is lower than that of the equivalent non-limiting case  $\approx -1.45 \times 10^{-15} [J]$ .

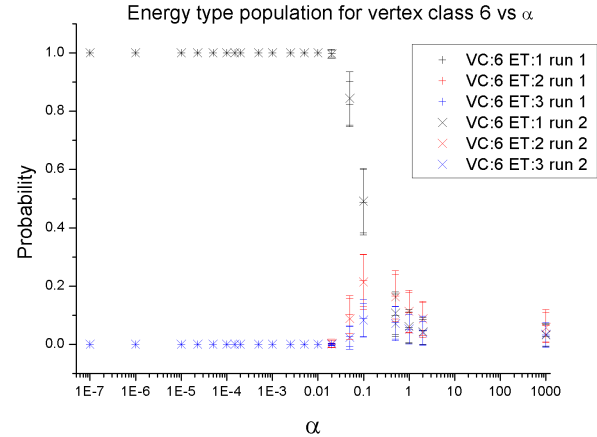


Figure 43: Evolution of the vertex class 6 population converge to have all vertices in the ground state

Over the course of the simulation, the population of vertex class 2 converges to have 110 members in the ground state and 185 in the first excited state. Furthermore vertex class 4 has all 46 members in the ground state, while vertex class 6 has all 20 members in the ground state.

## Conclusion

The vertex populations obtained from this simulation group seem to confirm the trend which was present in the previous Penrose simulations. The previous simulations were not able to successfully establish the exact statistics, however this may be due to the limited amount of simulation time available. With enough

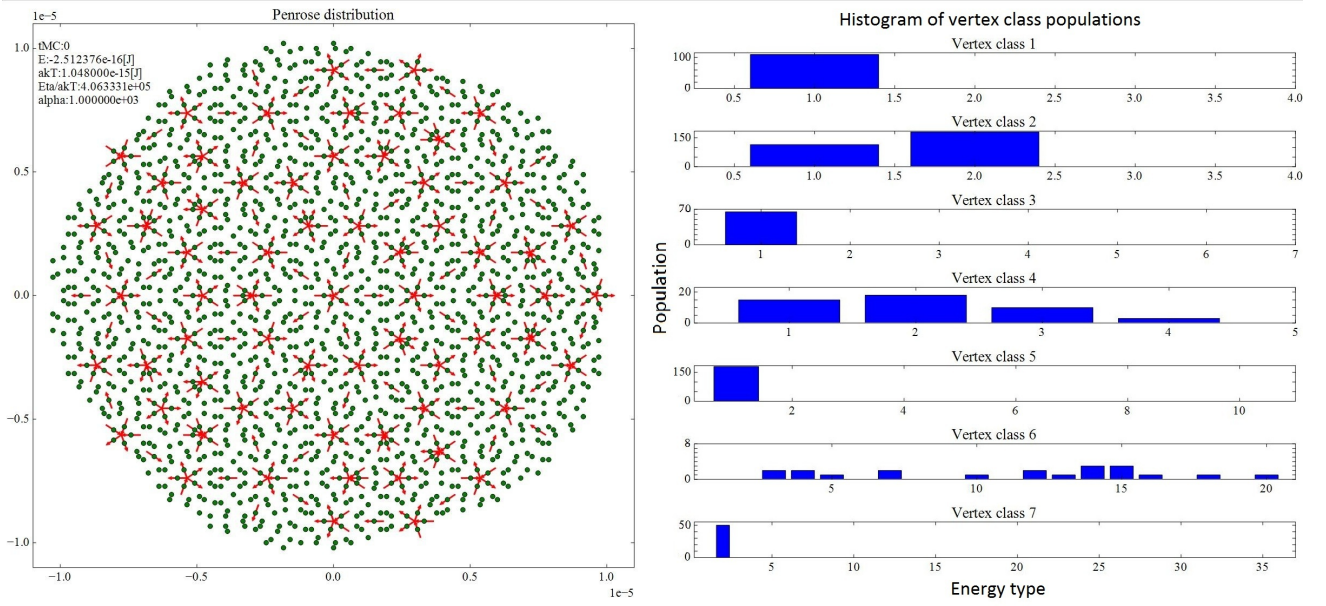


Figure 38: Distribution (left) and vertex population histogram (right) of a Penrose state with 1650 dipoles in its initial state with randomised polarities. Only the flippable vertices are displayed (coloured in red.) The energy of this initial state is  $-1.3571 \times 10^{-15} [J]$ , which is low compared to the initial states of the previous run but not unexpected if the skeleton mask forms a partial ground state.

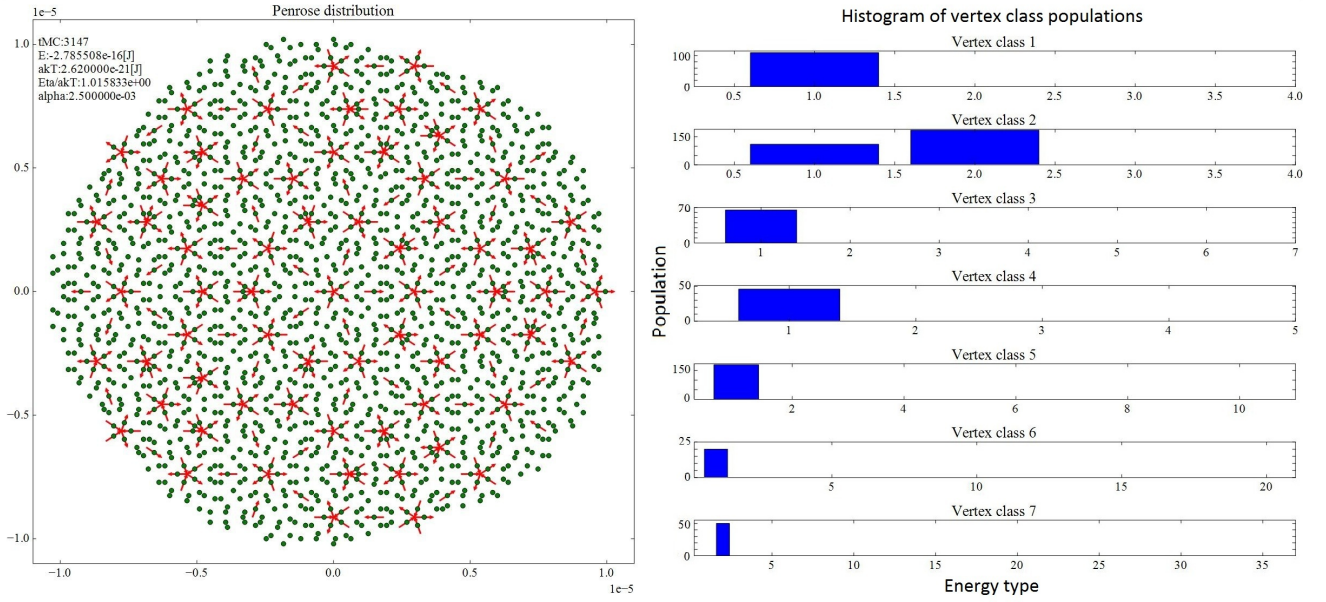


Figure 39: Distribution (left) and vertex population histogram (right) of a Penrose state with 1650 dipoles at MC step 3147. Again only the flippable dipoles are displayed (coloured in red.) Vertex classes 2, 4 and 6 have no vertices with population in the 3rd energy type, this is an indication that state is fairly well minimised. The energy of this state is  $-1.50464 \times 10^{-15} [J]$

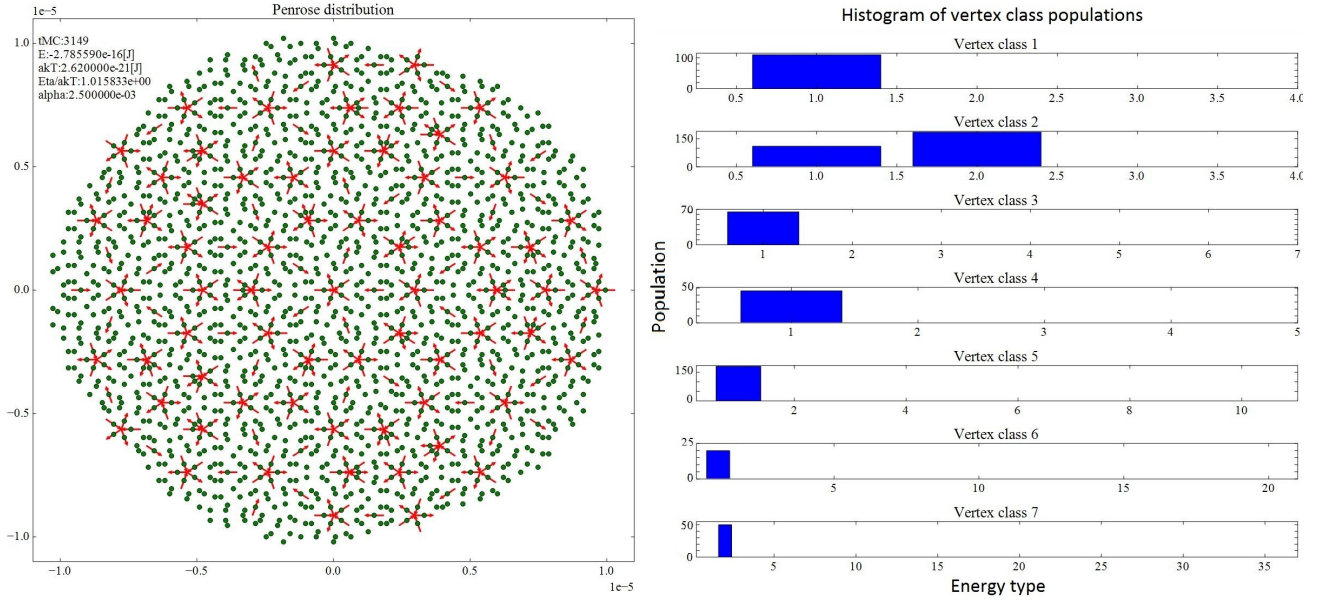


Figure 40: Distribution (left) and vertex population histogram (right) of a Penrose state with 1650 dipoles at MC step 3149. Again only the flippable dipoles are displayed (coloured in red.) Note that the vertex populations are the same as in figure 39 however the energy is in fact slightly lower at  $-1.50468 \times 10^{-15} [J]$ .

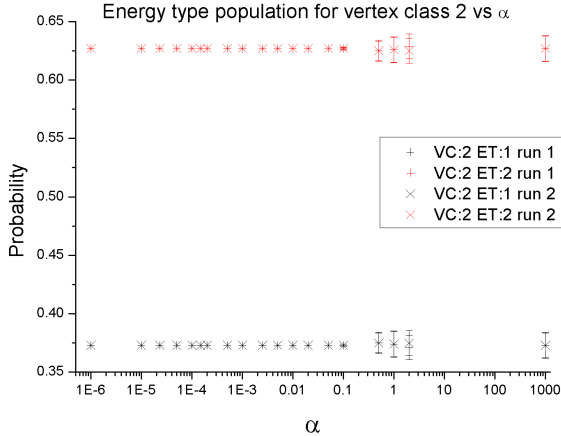


Figure 41: Evolution of the vertex class 2 population converge to have 62.5% in the first excited state and 37.5% in the group state.

simulation time I expect that the vertex populations would converge to these values.

The slight energy difference seen between the states depicted in figures 39 and 40 may seem trivial, however it is a significant result. The vertex classes have identical population distributions in these two states. With the presence of an energy difference, one can infer that long range interactions between the flippable dipoles play an important part in the lower energy region of the state space.

I cannot conclude that the state depicted in 40 is

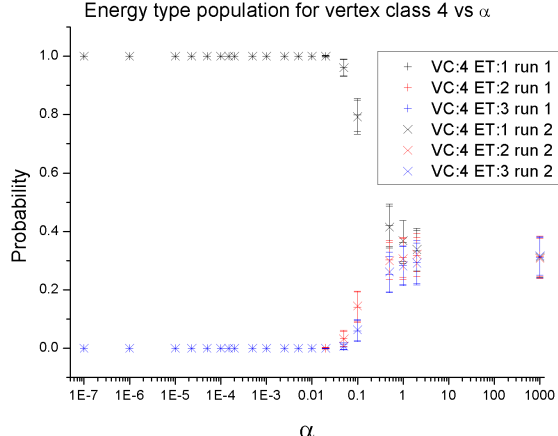


Figure 42: Evolution of the vertex class 4 population converge to have all vertices in the ground state.

the definitive ground state for the flippable islands. More time simulating this system would be required to get a definitive answer.

The lowest energy state found is not symmetric. If the true ground state is symmetric then due to the five fold symmetry and double degeneracy, the ground state would be ten fold degenerate. If the ground state is not symmetric then the degeneracy may be even higher.

## 0.4 Conclusion

It has been ascertained that very long simulation times are required, to make any significant head way in minimising frustrated systems of the Penrose flavour.

The issue of saturation has been a major problem in this project. Without knowledge as to the true dipole moment, it is hard to confirm any real world properties of the Penrose ASI but the methodology remains valid. The systematic errors induced by the saturation problem has skewed the heat capacity data and made determination of the true critical transition temperature impossible for now.

I believe enough data was gathered to conclude the distribution of vertex populations for the ground state configuration for a 1650 Penrose ASI. Nevertheless the limiting case MC simulation indicates, that even with the vertices populated in their ground state configuration, there is still plenty of room for further energy minimisation and thus the true ground state remains unknown. Long range interaction between the dipoles absent from the skeleton mask are truly significant and cannot be neglected.

## 0.5 Appendix

Heat capacity derivation:

$$C_v = \frac{\partial \langle E \rangle}{\partial T} = -\frac{\beta}{T} \frac{\partial \langle E \rangle}{\partial \beta} = \frac{\beta}{T} \frac{\partial^2 \ln Z}{\partial \beta^2} = \frac{\beta}{T} \frac{\partial}{\partial \beta} \left( \frac{1}{Z} \frac{\partial Z}{\partial \beta} \right) = \frac{\beta}{T} \left( \frac{1}{Z} \frac{\partial^2 Z}{\partial \beta^2} - \frac{1}{Z^2} \left( \frac{\partial Z}{\partial \beta} \right)^2 \right) = \frac{\beta}{T} (\langle E^2 \rangle - \langle E \rangle^2)$$
$$C_v = \frac{\beta}{T} (\langle E^2 \rangle - \langle E \rangle^2)$$

Table 4: Square spin ice, Stage duration and Subsample for run 1 vs  $\alpha$ 

Alpha	Stage duration	Subsample length	Number of subsamples
1000	628	124	5
100	683	135	5
5	794	157	5
2	727	144	5
1.5	731	145	5
1	792	157	5
0.75	759	150	5
0.5	402	79	5
0.25	2691	537	5
0.125	697	138	5
0.0625	1289	256	5

Table 5: Square spin ice, Stage duration and Subsample for run 2 vs  $\alpha$ 

Alpha	Stage duration	Subsample length	Number of subsamples
1000	638	126	5
100	721	143	5
5	759	150	5
2	737	146	5
1.5	762	151	5
1	772	153	5
0.75	789	156	5
0.5	411	81	5
0.25	2725	544	5
0.125	818	162	5
0.0625	1190	237	5

Table 6: 720 dipole Penrose spin ice, Stage duration and Subsample for run 1 vs  $\alpha$ 

Alpha	Stage duration	Subsample length	Number of subsamples
1000	659	81	8
2	657	81	8
1.9	696	86	8
1.8	886	109	8
1.6	767	94	8
1.4	2096	261	8
1.2	734	90	8
1	893	110	8
0.8	860	106	8
0.6	1183	146	8
0.4	865	107	8
0.3	1428	177	8
0.25	950	117	8
0.2	1611	200	8
0.15	1023	126	8
0.1	2052	255	8
0.09	1133	140	8
0.085	1428	177	8
0.08	1544	192	8
0.075	1324	164	8
0.07	1416	176	8
0.065	1429	177	8
0.06	2114	263	8
0.05	1683	209	8
0.025	1254	155	8
0.01	814	100	8

Table 7: 720 dipole Penrose spin ice, Stage duration and Subsample for run 2 vs  $\alpha$ 

Alpha	Stage duration	Subsample length	Number of subsamples
1000	646	79	8
2	651	80	8
1.9	681	84	8
1.8	866	107	8
1.6	749	92	8
1.4	2063	256	8
1.2	702	86	8
1	884	109	8
0.8	840	104	8
0.6	1161	144	8
0.4	865	107	8
0.3	1394	173	8
0.25	919	113	8
0.2	1580	196	8
0.15	1017	126	8
0.1	1992	248	8
0.09	1104	137	8
0.085	1487	184	8
0.08	1417	176	8
0.075	1291	160	8
0.07	1388	172	8
0.065	1390	172	8
0.06	2069	257	8
0.05	1636	203	8
0.025	1235	153	8
0.01	1472	183	8

Table 8: 1650 dipole Penrose spin ice stage durations

Alpha	Stage duration run 1	Stage duration run 2	Stage duration run 3
1000	639	637	637
1.8416	704	702	694
1.4599	594	610	606
1.2118	621	627	623
0.72233	848	868	850
0.34924	894	896	907
0.17462	838	847	835
0.09655	1515	1541	1555
0.015448	835	848	797
0.048275	740	751	744
0.015448	835	848	797
0.01116	1086	1107	1090
0.008298	748	761	750
0.007882	655	669	655
0.005715	640	652	641
0.003862	641	652	645

Table 9: 1650 dipole Penrose spin ice, limited MC, stage durations

Alpha	Stage duration run 1	Stage duration run 2
1000	454	453
2	127	123
1	386	390
0.5	223	219
0.1	349	354
0.05	110	113
0.02	403	410
0.01	328	328
0.005	246	249
0.0025	545	547
0.001	29	30
0.0005	109	112
0.0002	69	69
0.0001	46	45
0.0005	109	112
0.0002	69	69
0.00015	15	15
0.0001	46	45
0.00005	8	8
0.000023	24	25
0.00001	18	17
0.000001	42	42
0.0000001	30	30

Table 10: Vertex class 1→6 energy type degeneracies

Vertex class	Code	Energy Type	Degeneracy	Probability
1	69	3	2	0.25
		2	2	0.25
		1	4	0.5
		Total	8	1
		3	2	0.25
		2	4	0.5
		1	2	0.25
		Total	8	1
2	73	6	2	0.125
		5	4	0.25
		4	2	0.125
		3	4	0.25
		2	2	0.125
		1	2	0.125
		Total	16	1
		4	2	0.0625
3	85	3	10	0.3125
		2	10	0.3125
		1	10	0.3125
		Total	32	1
		10	2	0.0625
		9	2	0.0625
		8	4	0.125
		7	4	0.125
4	341	6	4	0.125
		5	4	0.125
		4	4	0.125
		3	2	0.0625
		2	2	0.0625
		1	4	0.125
		Total	32	1
		20	2	0.03125
5	155	19	2	0.03125
		18	4	0.0625
		17	4	0.0625
		16	2	0.03125
		15	2	0.03125
		14	4	0.0625
		13	4	0.0625
		12	4	0.0625
6	343	11	4	0.0625
		10	4	0.0625
		9	4	0.0625
		8	4	0.0625
		7	4	0.0625
		6	2	0.03125
		5	2	0.03125
		4	4	0.0625
7	171	3	2	0.03125
		2	4	0.0625
		1	2	0.03125
		Total	64	1

Table 11: Vertex class 7 energy type degeneracies

Vertex class	Code	Energy Type	Degeneracy	Probability
7	375	36	2	0.015625
		35	2	0.015625
		34	4	0.03125
		33	4	0.03125
		32	4	0.03125
		31	4	0.03125
		30	4	0.03125
		29	4	0.03125
		28	4	0.03125
		27	4	0.03125
		26	4	0.03125
		25	4	0.03125
		24	4	0.03125
		23	4	0.03125
		22	2	0.015625
		21	2	0.015625
		20	4	0.03125
		19	4	0.03125
		18	2	0.015625
		17	4	0.03125
		16	4	0.03125
		15	4	0.03125
		14	4	0.03125
		13	4	0.03125
		12	2	0.015625
		11	4	0.03125
		10	4	0.03125
		9	4	0.03125
		8	4	0.03125
		7	4	0.03125
		6	4	0.03125
		5	4	0.03125
		4	4	0.03125
		3	2	0.015625
		2	4	0.03125
		1	2	0.015625
	Total		128	1

# Bibliography

- [1] . Permalloy material overview, 2013.
- [2] K. Binder and A. P. Young. Spin glasses: Experimental facts, theoretical concepts, and open questions. *Rev. Mod. Phys.*, 1986.
- [3] R. Moessner C. Castelnovo and S.L. Sondhi. Magnetic monopoles in spin ice. *Nature*, 2008.
- [4] Michael R. Chernick. The jackknife: a resampling method with connections to the bootstrap. *Wiley Interdisciplinary Reviews: Computational Statistics*, 4(2):224–226, 2012.
- [5] Jie Li Cristiano Nisoli and Xianglin Ke. Effective temperature in an interacting vertex system: Theory and experiment on artificial spin ice. *PHYSICAL REVIEW LETTERS*, 2010.
- [6] N.G. de Bruijn. Algebraic theory of penroses non-periodic tilings of the plane. *Indagationes mathematica*, 1980.
- [7] W. F. Giaque and J. W. Stout. the entropy of water and the third law of thermodynamics. heat capacity of ice from 15k to 273k. *J. Am. Chem. Soc.*, 1936.
- [8] Michel J.P. Gingras. Spin ice review paper. *ARXIV*, 2009.
- [9] J. Hafner and M. Krajčí. Formation of magnetic moments in crystalline, quasicrystalline, and liquid al-mn alloys. *Phys. Rev. B*, 57:2849–2860, Feb 1998.
- [10] Riccardo HERTEL. Thickness dependence of magnetization structures in thin permalloy rectangles. *Zeitschrift für Metallkunde*, 93(10):957–962, 2002.
- [11] Erik Huss. The royal swedish academy of sciences. scientific background on the nobel prize in chemistry 2011: The discovery of the quasicrystal, 2011.
- [12] T Janssen. Crystallography of quasi-crystals. *Acta Crystallographica Section A: Foundations of Crystallography*, 42(4):261–271, 1986.
- [13] R Kubo. The fluctuation-dissipation theorem. *Reports on Progress in Physics*, 29(1):255, 1966.
- [14] David P. Landau and Kurt Binder. *A guide to Monte Carlo Simulations in Statistical Physics*. , .
- [15] D. Levis, L. F. Cugliandolo, L. Foini, and M. Tarzia. Thermal phase transitions in Artificial Spin-Ice. *ArXiv e-prints*, February 2013.
- [16] Norberto Majlis. *The Quantum Theory of Magnetism*.
- [17] Roderich Moessner and Arthur P. Ramirez. Geometrical frustration. *Physic today*, 2006.
- [18] Wayne M Patrick, Andrew E Firth, and Jonathan M Blackburn. User-friendly algorithms for estimating completeness and diversity in randomized protein-encoding libraries. *Protein engineering*, 16(6):451–457, 2003.
- [19] Linus Pauling. The structure and entropy of ice and of other crystals with some randomness of atomic arrangement. *J. Am. Chem. Soc.*, 1935.
- [20] R. F. W. Pease. Electron beam lithography. *Contemporary Physics*, 22(3):265–290, 1981.
- [21] J. Sethna. *Statistical Mechanics: Entropy, Order Parameters, and Complexity*. Oxford master series in statistical, computational, and theoretical physics. OUP Oxford, 2006.
- [22] D. Shechtman and I. Blech. Metallic phase with long-range orientational order and no translational symmetry. *PHYSICAL REVIEW LETTERS*, 1984.
- [23] E. Y. Vedmedenko, U. Grimm, and R. Wiesendanger. Interplay between magnetic and spatial order in quasicrystals. *Philosophical Magazine*, 86(6-8):733–739, 2006.
- [24] D.J. Wales. *Energy Landscapes*, volume 73 of *Les Houches - Ecole d'Ete de Physique Theorique*. Springer Berlin Heidelberg, 2001.
- [25] R.F. Wang and C.Nisoli. Artificial spin ice in a geometrically frustrated lattice of nanoscale ferromagnetic islands. *Nature*, 2006.

- [26] EJW Whittaker and RM Whittaker. Some generalized penrose patterns from projections of n-dimensional lattices. *Acta Crystallographica Section A: Foundations of Crystallography*, 44(2):105–112, 1988.
- [27] A. Yamamoto and K. N. Ishihara. Penrose patterns and related structures. II. Decagonal quasicrystals. *Acta Crystallographica Section A*, 44(5):707–714, Sep 1988.
- [28] Akiji Yamamoto and KN Ishihara. Penrose patterns and related structures. ii. decagonal quasicrystals. *Acta Crystallographica Section A: Foundations of Crystallography*, 44(5):707–714, 1988.
- [29] David .J. Sellmyer Yi Liu and Daisuke Shindo, editors. *Handbook of Advanced Magnetic Materials*. Springer, 2006.